UC Irvine
UC Irvine Electronic Theses and Dissertations

Title
Modal and Harmonic Simulation Studies of Three Fourier Horn Asymmetric Ultrasonic Atomizer Nozzles

Permalink
https://escholarship.org/uc/item/2vz1d9sg

Author
Maduzia, James Frank

Publication Date
2014

Peer reviewed|Thesis/dissertation

eScholarship.org Powered by the California Digital Library
University of California

UNIVERSITY OF CALIFORNIA,
IRVINE

Modal and Harmonic Simulation Studies of Three Fourier Horn Asymmetric Ultrasonic Atomizer Nozzles

THESIS

submitted in partial satisfaction of the requirements
for the degree of

MASTER OF ENGINEERING

in Electrical and Computer Engineering

by

James Maduzia

Thesis Committee:
Professor Chen Tsai, Chair
Professor Chin C. Lee
Professor G. P. Li

2014

© 2014 James Maduzia

TABLE OF CONTENTS

LIST OF FIGURES

LIST OF TABLES

ACKNOWLEDGMENTS

I would like to thank Chancellor's Professor Chen S. Tsai for all his help and support during my time as a graduate student both financially and personally. He clearly went above and beyond in his efforts to support my research career. I also want to thank Professor Shirley Tsai for her abundant assistance and direction as well. To Dr. Rong Wei Mao I want to acknowledge his extensive help in helping me learn and understand the concepts of my research. I also want to thank Shih-Kai Lin, Yun Zhu, and Eric Fan-Tsen Chien for their assistance in various aspects of my research project. I want to thank Kai-Hung Chi for general theoretical discussions concerning my project. I would like to also thank Grace Kim and my Lord and Savior Jesus Christ for always being there for me. Lastly the financial support provided by the NIH and Shih-Lin Electrics, U.S.A are also gratefully acknowledged.

ABSTRACT OF THE DISSERTATION

Modal and Harmonic Simulation Studies of Three Fourier Horn Asymmetric Ultrasonic Atomizer Nozzles

By

James Maduzia

Master of Engineering in Electrical and Computer Engineering

University of California, Irvine, 2014

Professor Chen Tsai, Chair

A method for comparing related nozzle designs possessing widths proportional to their frequencies over a broad frequency range is presented and utilized on asymmetric multiple Fourier nozzle designs. The underlying causes of the frequency dependent performance of the nozzle designs are explored and compared. Based on this knowledge, a better understanding of the operation of the nozzles is obtained. From this understanding, nozzle designs intended to operate at higher frequencies can be built in a more effective manner.

Chapter 1

Introduction

The multiple Fourier horn ultrasonic atomization nozzle project has steadily evolved since its inception into an extremely promising new technology [1] - [7]. Currently it is poised to revolutionize the medical pulmonary drug delivery field. This technology also has the potential to make an impact in the field of nanotechnology .

The purpose of the multiple Fourier horn ultrasonic nozzle is to create a mono-disperse aerosol directly from a liquid. Its unique design can accomplish this without fragile mesh structures or mechanical parts. The droplet size of this aerosol is directly determined by the operational frequency of the nozzle. Since the nozzle can potentially be designed to operate at any frequency within megahertz (MHz) range, this type of nozzle will be ideal for any application that requires a precise monodisperse aerosol of a specific size within the micron regime. The fundamental physical mechanism responsible for the creation of these individual droplets in such a highly consistent manner is known as the temporal instability of the Faraday wave [6].

The Faraday wave is a standing capillary wave formed on the free surface of a liquid layer undergoing a periodic vertical acceleration. This was first observed in 1831 by

Michael Faraday [8] when he subjected a flexible membrane supporting a liquid layer to just such an acceleration. Once the amplitude of acceleration reaches a critical value the waves are formed.

What Faraday did not see at the time was that if this critical amplitude is maintained the waves will eventually break up and and eject droplets. This phenomenon is known as the Faraday instability from wave formations. The connection between the Faraday wave and droplet formation was first made by Tsai's theory. Because the Faraday wave is distributed across the entire free surface of the liquid layer and possesses a uniform wavelength, the droplets created via Faraday instability will also be created and ejected in a uniform manner. The size of the droplets formed in such a manner were empirically shown to be proportional to the wavelength of the Faraday waves. This is initially given by the relationship updated by Lang in 1962 [9]:

$$D_p = 0.34\lambda \tag{1.1}$$

The relationship between the operational frequency of the nozzle and the wavelength of the capillary (Faraday) wave is predicted by the Kelvin equation:

$$\lambda = (\frac{8\pi\sigma}{\rho})^{1/3}(\frac{1}{f^{2/3}}) \tag{1.2}$$

Here ρ and σ are the density and surface tension of the liquid respectively. From the Kelvin equation Equation (1.2) and Lang's empirical relationship Equation (1.3) the size of the droplet produced by the multiple Fourier horn nozzle design can be predicted. However, the detailed theory developed by Tsai predicts a droplet diameter given by:

$$D_p = 0.4\lambda \tag{1.3}$$

This updated theoretical droplet size prediction has verified the diameter of droplets produced experimentally by multiple Fourier horn nozzles.

In 1883 Lord Rayleigh repeated Faraday's original experiment in detail and rigorously characterized the observed results mathematically [10]. Immediately afterward the Faraday wave was effectively relegated to a scientific curiosity for a hundred years. Starting in the early 1990's several authors revisited the concept by undertaking studies of the phenomenon at driving frequencies from 6 Hz to 50Khz [12] -[19]. Even up to this time, no explicit theoretical relationship had been established between Faraday instability and atomization. This link was made by Tsai et al. 2010 [3] after they had already accomplished atomization in the MHz regime using a multiple Fourier horn nozzle prototype with a central channel Tsai et al. 2006 [1].

In order to achieve temporal Faraday Wave instability, the engineering challenge is to design an acoustic amplifier that can reach the necessary critical amplitude with satisfactory power requirements and stellar reliability. Such an acoustic amplifier in general is a solid bulk possessing a unique profile shape which causes compression or "sound" waves entering it at its base to obtain a significant increase in amplitude upon arrival at its tip. This bulk typically takes the shape of a horn, and they are often referred to as such.

The problem of achieving Faraday wave instability has been addressed by Tsai et al. by employing an amplifier design with a unique profile first derived theoretically by Eisner in his 1963 work entitled "Design of Sonic Amplitude Transformers for High Magnification" [11]. Equation 13f of Eisner's paper, recounted here as Equation (1.4), relates the longitudinal position along the horn's x-dimension with the rectangular

cross-sectional area of the profile in the y-z plane at that point.

$$\frac{dlnA}{d(cos\pi X)} = \frac{(4-\gamma^2)(\gamma^2+\alpha_{42}) - \mu(9-\gamma^2)(\gamma^2-1)cos\pi X - (16-\gamma^2)\alpha_{42}cos^2\pi X}{\mu(3-\gamma^2) - 2(\gamma^2+2\alpha_{42})cos\pi X + 3\mu(\gamma^2-1)cos^2\pi X + 4\alpha_{42}cos^3\pi X} \quad (1.4)$$

This amplification profile is aptly labeled as a "Fourier" profile since Eisner deduced the shape from a wave function described by a 4th order Fourier series. Depending on the parameters of γ, and α_{42} set in Equation (1.4), a particular horn's magnification can be as large as a factor of 2.

Invented by Tsai [5], the multiple Fourier horn nozzle, as its name suggests, utilizes several of these amplitude transformers. In order to reach the critical amplitude required for free surface breakup via temporal Faraday wave instability, several Fourier horns are arranged from base to tip in series.

The liquid layer to be atomized in our case rests on the tip of the terminal horn. Therefore, the end face of this terminal, or "tip", horn possesses the exact same functionality as the vibrating elastic surfaces used by Faraday and the glass plate used by Rayleigh: it is the support by which the oscillations are introduced into the liquid. If each horn possesses the maximum internal magnification mentioned in the last paragraph, then the final displacement of the tip of a three horn nozzle would be subjected to is 8 times the amplitude of the original wave.

Tsai's method of constructing the nozzles utilizes silicon crystal wafers. These wafers are readily available and inexpensive due to their extensive use in the silicon microchip industry as integrated circuit substrates. Such wafers can be found in standard thicknesses of 400 and 800 microns. The silicon crystal wafer's combination of bulk and shear modulus characterize it as an ideal material for sustained transmission of longitudinal compression waves. Since silicon crystal by itself does not possess a sufficiently large electromechanical coupling coefficient for efficient conversion between

electrical and mechanical (vibration or sound) energy, a plate of piezoelectric material such as PZT is required for the conversion. The longitudinal vibrations amplified by the Fourier horns of the nozzle initially originate from electro-mechanical transduction provided by lead zirconate titanate (PZT) piezoelectric transducer elements connected to a MHz A/C signal.

The nozzle is etched from the wafers using the dry anisotropic Bosch process. This is a micro-electromechanical system (MEMS) fabrication method which has widely proven to be economical and precise. The result of the etching process produces the nozzle connected to a support manifold. The nozzle itself consists of the Fourier horn series with a rectangular segment at its base. This segment is known as the"driving section". The PZT plate transducer elements are bonded to the driving section of the nozzle. These vibrations are immediately transfered into the driving section through the bond between piezoelectric plate and the silicon wafer before being amplified by the series of Fourier horns.

The combination of the driving section and the Fourier horn series makes up what is referred to as the "nozzle". The nozzle is connected to the support manifold by what are called the "nodal supports". Each individual amplifier horn and driving section is supported by the manifold via a nodal bar on each side. An example of a single drive nozzle model is shown in Figure 1.1.

As the vibration propagates from the driving section it encounters the base of the first Fourier horn amplitude transformer. After traveling the length of this horn, the amplitude of the original vibration will have been significantly increased governed by the magnification defined by Eisner's equation [equ.4].

The desired vibration is that of a purely longitudinal vibration. This desired mode shape will also be referred to as the "operational" mode of the nozzle. This vibration

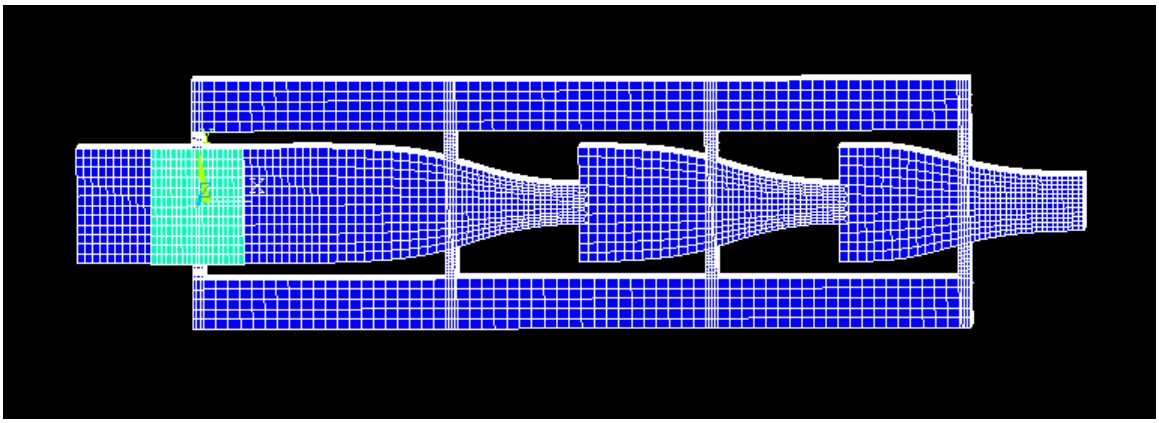

Figure 1.1: Three Fourier Horn Nozzle Model with Support Manifold

displaces the silicon wafer of the nozzle soley along the longitudinal (x-axis) axis of the nozzle. This mode will result in a standing longitudinal compression wave will be set up in the nozzle. For this wave to be obtained, the nodal support bars must match up precisely with the nodes of the standing wave, hence their name.

One proven nozzle construction design consists of two 400 micron wafers bonded together. In order to achieve a design with an element on each side, each element would first be bonded to a nozzle etched out of a 400 micron wafer and then two of these nozzle halves would be bonded together to complete the nozzle. This "double bonded" design is also referred to as a "symmetric" or "dual drive symmetric" design (SDD).

In contrast, the "asymmetric" nozzle design consists of a single 800 micron thick silicon wafer with piezoelectric element(s) bonded to only one side. Having the PZT elements bonded on each side of the symmetric nozzle facilitates the longitudinal vibrations to travel down to the tip of the multiple Fourier horn nozzle as evenly as possible since the vibrations are input to the silicon bulk wafer in a balanced and symmetrical fashion. If these vibrations were not balanced, there would theoretically be more twisting of the nozzle which would lead to more stress and impedance potentially resulting in a significant reduction in the nozzle's performance and reliability.

The drawback of the symmetric nozzle design is the fact that it takes a very intensive extra step of having to bond the two wafers together. While it is assumed that the asymmetric configuration will not be able to fully match the performances of a comprable symmetric design, a major goal of this research will be to determine whether it is a viable alternative.

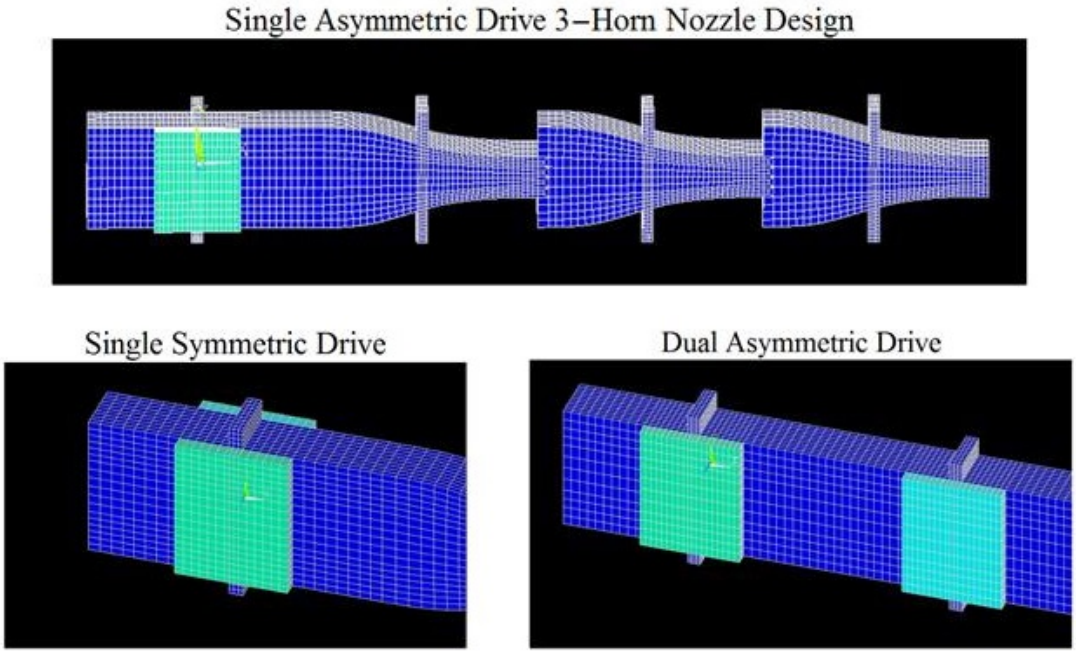

Figure 1.2: 1.0MHz Nozzle Design driving section comparisons

In my research, I primarily focus on two versions of the 3 horn asymmetric nozzle design: the asymmetric single drive (ASD) and asymmetric dual drive (ADD) design. The symmetric dual drive (SDD) design is also included as a comparison at limited frequencies. A visual comparison of the ANSYS mesh models of these three different nozzle designs can be found in Figure 1.2. The Fourier horn section of all three of these nozzle designs is identical. The only unique aspect of each of these nozzles is the configuration of the piezoelectric elements and number of driving sections.

The immediate goal of this research is to improve the performance of the asymmetric

nozzle designs. In spite of their drawbacks, the asymmetric nozzle designs may be suitable for specific applications that are less demanding in terms of absolute performance. I have devoted my thesis to characterizing these asymmetric nozzle designs with operational frequencies ranging from 0.9MHz to 2.3MHz. The droplet diameters produced by nozzles operating within this range aligns with the center of the droplet sizes for optimum absorption by the alveoli in the lungs. A nozzle designed to operate in this frequency range thus is ideally suited to be the active component of a next-generation inhalation drug delivery system.

The current theory describing the Faraday wave developed by C.S Tsai [6] is an approximation that linearizes the differential governing equations and conditions of Faraday's initial problem. This approximation is accurate provided that the amplitude of the Faraday waves are small compared to the dimensions of the free surface on which they are constrained. In this case, the free surface is determined by the end face of the terminal Fourier horn. Since the nozzles must continually shrink in order to accommodate ever higher frequencies, this approximation will eventually cease to describe the diameters of the droplets they produce. Experimental results showed here that the linear theory matched the droplets produced by a three Fourier horn nozzle operating at frequencies up to 1.5MHz [2]. Droplets formed by nozzles operating at significantly higher frequencies will need to be described by a non-linear theory.

Once Tsai's linear Faraday instability theory is updated to include non-linear effects, it will need to be verified using the experimental results. The only way to obtain these results will be to design and operate nozzles at frequencies well above 1.5MHz. Effective methods of designing such nozzles will be necessary in order to produce these nozzles able to create droplets with small enough diameters. These methods will rely on better understanding the underlying causes of the behavior of the nozzle

designs.

The overall intent of this study is to characterize the asymmetric nozzle designs over the 0.9MHz to 2.3MHz broad frequency range as thoroughly as possible so that their fundamental physical responses can be explored and resolved. Such an understanding will be valuable in guiding the design of future nozzles that will be able to result in Faraday wave instability above the linearized regime.

Chapter 2

Data and Results

The simulation studies featured in this thesis are designed to reveal the underlying causes behind the behavior of the asymmetric multiple Fourier horn nozzles. This was done by searching for correlations between the frequency dependent harmonic and modal behavior of these nozzle designs over the entire broad frequency range. The goal in doing so was to test a hypothesis stating that a non-longitudinal neighbor mode will affect the operation of the nozzle if it starts to encroach on its operational frequency. One of the expected effects of this interference is an increase in the harmonic results, specifically that of Z-normal stress, power, and voltage.

This type of simulation comparison method consists of building a set of nozzles of the same design which are scaled to operate at regular intervals within the overall frequency range while all other aspects of their design are kept as comparable as possible. The method of constructing such a set of related nozzles consists of designing nozzles that have widths which are inversely proportional to their operational frequencies positioned at intervals over a large frequency range. Each of the nozzle component mesh models, the piezoelectric plate, driving section, and Fourier horn would be de-

signed to match that width before being simulated individually. The length of each of these components would be adjusted until they all matched the target frequency independently. Finally, all of these individual components will be combined together to model one of the nozzles of the comparison set before it is optimized via its nodal support positions to facilitate the standing wave of the desired longitudinal vibration at that particular frequency.

The data is extracted from these nozzle designs using two separate ANSYS analysis procedures. The modal analysis step first finds the frequencies of all of the vibration modes of the extended nozzle structure. While obtaining the frequency of the pure longitudinal vibrational mode is required to for the harmonic analysis, the remaining "non-longitudinal" modes are extensively utilized in the comparison. These neighbor modes would first be identified by their displacement contour shape before being individually tracked against the pure longitudinal mode of nozzle designs. The differences between the frequencies of each non-longitudinal modes and the operational frequency of the corresponding nozzle were calculated and this difference was plotted over the entire frequency of the comparison set. This is referred to as a neighbor mode track plot.

The first design compared in this way is the ASD design. The ADD set was then built by adding a second driving section to this first set. The various other broad frequency comparison sets created for this research are further modifications of these initial ASD and ADD sets.

The interference theory is tested here by looking for correlations between the harmonic and modal data sets. Various modified data sets are introduced within such a study get an idea of how the modification affects the nozzle design over the entire frequency range. At limited frequencies I will also attempt to compare these designs to symmetric SDD designs.

2.1 Initial Harmonic Results for Single and Dual Drive Nozzles

I found that both the initial ASD and ADD nozzle sets appeared to follow the same overall trend in their harmonic data. This was a linear increase which transitioned into an exponential increase quickly taking the stress and voltage data outside of an acceptable range even though the mode shape of the final optimized nozzles found by ANSYS kept a tenuous grasp on the longitudinal mode up to 1.6MHz. Past this frequency however, the longitudinal mode shape of the nozzle clearly failed. After the about 1.9MHz, the harmonic data was later seen to fall back down. Only the plot of the Z-normal stress of this comparison is presented in this section. The remaining harmonic plots of voltage Figure A.1, power Figure A.2 and impedance Figure A.3 can be found in Appendix A.

The Z-normal stress is compared between the ASD and ADD nozzles over the frequency range from 0.9MHz - 2.3MHz in Figure 2.1. In the range from 0.9MHz to about 1.6MHz, the dual drive nozzle design was superior to the single drive version, but only marginally. This superiority was demonstrated in the dual drive nozzle as a lower required voltage and z-normal stress at the expense of slightly higher power required to run the nozzle. Past 1.6MHz, the two stress values of the two designs start to diverge from each other with the dual drive having a significantly lower value. However, for both of the nozzle designs, the stress at these frequencies was already well beyond the acceptable level. In order for a nozzle to be considered for fabrication it must be generally have a stress rating under 4 [MPa]. Therefore it is clear that both the ASD and ADD nozzle designs do not give acceptable results above about 1.4MHz. In spite of this, it is still noteworthy that at 2.2MHz, just after the stress seems to go back to the initial linear increase, the dual and single values once again

match up very closely to each other.

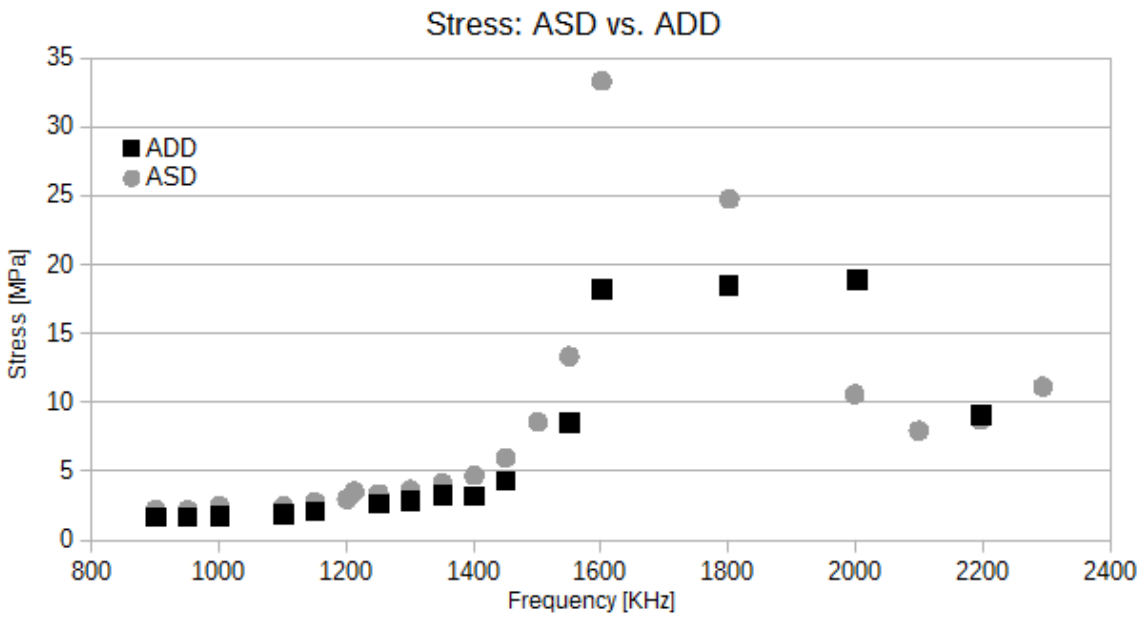

Figure 2.1: ASD vs. ADD Stress Comparison

The voltage plot, Figure A.1, appears to follow an overall path very similar to that of the stress except for a couple notable differences. First of all, although the voltage values transition from a linear increase to an exponential one, they both drop down much more sharply at the 1.8MHz data point before rising again for a second peak. In fact, you will see that the voltage at this point is actually significantly lower than many of the points in the initial linear section. This dip in the voltage is not mirrored in the corresponding stress data point for 1.8MHz nozzle although this point does appear to be an inflection point of the impedance values. Another interesting aspect of this comparison was that although the stress, and even the power, returned to its original linear increase after the central region, the voltage did not, even though it had initially increased in the same way between 0.9MHz and 1.3MHz. Instead, the voltage began a slow linear decrease from 2.0MHz to 2.3MHz. It is also interesting to note that like stress comparison, the voltage between the dual and single drives is far closer at the two extremes of the frequency range while diverging in the middle.

The power comparison between the dual and single drives designs in Figure A.2 tracks more similarly to the stress than the voltage did. The power for the dual drive is almost always greater than that of the single drive but this relationship does not hold at the beginning of the exponential spike at the 1.55MHz and 1.6MHz frequency points. The reason for this is not known. Just like the stress and voltage, the power data also diverges the most in this central region while converging back together at the higher frequencies once again confirming the trend.

The impedance appears to first follow a smooth and uninterrupted path until 1.8MHz where an inflection is seen. Then the two values then diverge drastically with the value of the dual drive far higher than that of the single drive at 2.0MHz. This behavior seems especially remarkable in light of the typically subdued behavior of the impedance. While this may be an anomalous outlier point due to inconsistent optimization of the 2.0MHz, a much more likely explanation is that it has to do with the intersection of the second pinch mode exactly at this point.

In general, the trends of the harmonic data of both of these two initial asymmetric comparison sets showed the same overall frequency dependent response in stress: a linear increase which turned into an exponential one around 1.4MHz. These two different regions are what I will refer to as the "linear" and "exponential" regimes. Throughout much of my research, the ASD and ADD nozzle sets were only completed up to about 1.6MHz where the nozzle designs started to fail due to stress accumulation. Later, once higher frequency designs were completed, the harmonic stress data was seen to return to the exact same linear increase seen initially. Therefore, the exponential increase will later be referred to as the "central stress spike" regime which covers the range from about 1.5MHz to 2.0MHz.

2.2 Initial ASD Modal Study

The first mode identified was named based on its appearance. The "snakey" mode possesses wavy appearance in the x-y plane. Its shape and mode tracks are cataloged in Figure 2.2. There were also four other mode classes that I identified and tracked over the broad frequency range of the ASD set. I called these modes based on their appearance. All of these interesting mode tracks are cataloged Appendix B in Figure B.4, Figure B.5 Figure B.6, and Figure B.7. Here, like in Figure 2.2, a screen capture of their X-component displacement contour plot is displayed alongside the mode track data of that shape over the entire frequency range from 0.9 MHz to 2.3MHz. For a clear understanding of the interaction of these neighbor modes with the nozzle, I would need to plot them against the harmonic data. This was done in this thesis by plotting the harmonic Z-stress value along with the mode tracks of all the neighbor modes in Figure 2.3. The pinch mode was the only full piezo-mode that was seen in the ASD modal data. All the rest of the vibration x-component displacement shapes recounted here appeared to originate in the nozzle body

Here I have plotted the selected modal data over the entire frequency range of 0.9MHz - 2.3MHz after first identifying and cataloging the most relevant and clearly distinguished neighbor modes by their shape. Here I will also differentiate between the mode types that seem to have the most potential for interfering with the operation of the nozzle and those that do not appear to have any effect. The tracks of the interference candidate modes are then plotted in direct comparison with the ASD scaled set stress data.

The track of the "snakey" non-longitudinal neighbor mode along with its x-component displacement contour screen capture is displayed in Figure 2.2. This was the first major non-longitudinal neighbor mode that I was able to find a clearly defined path

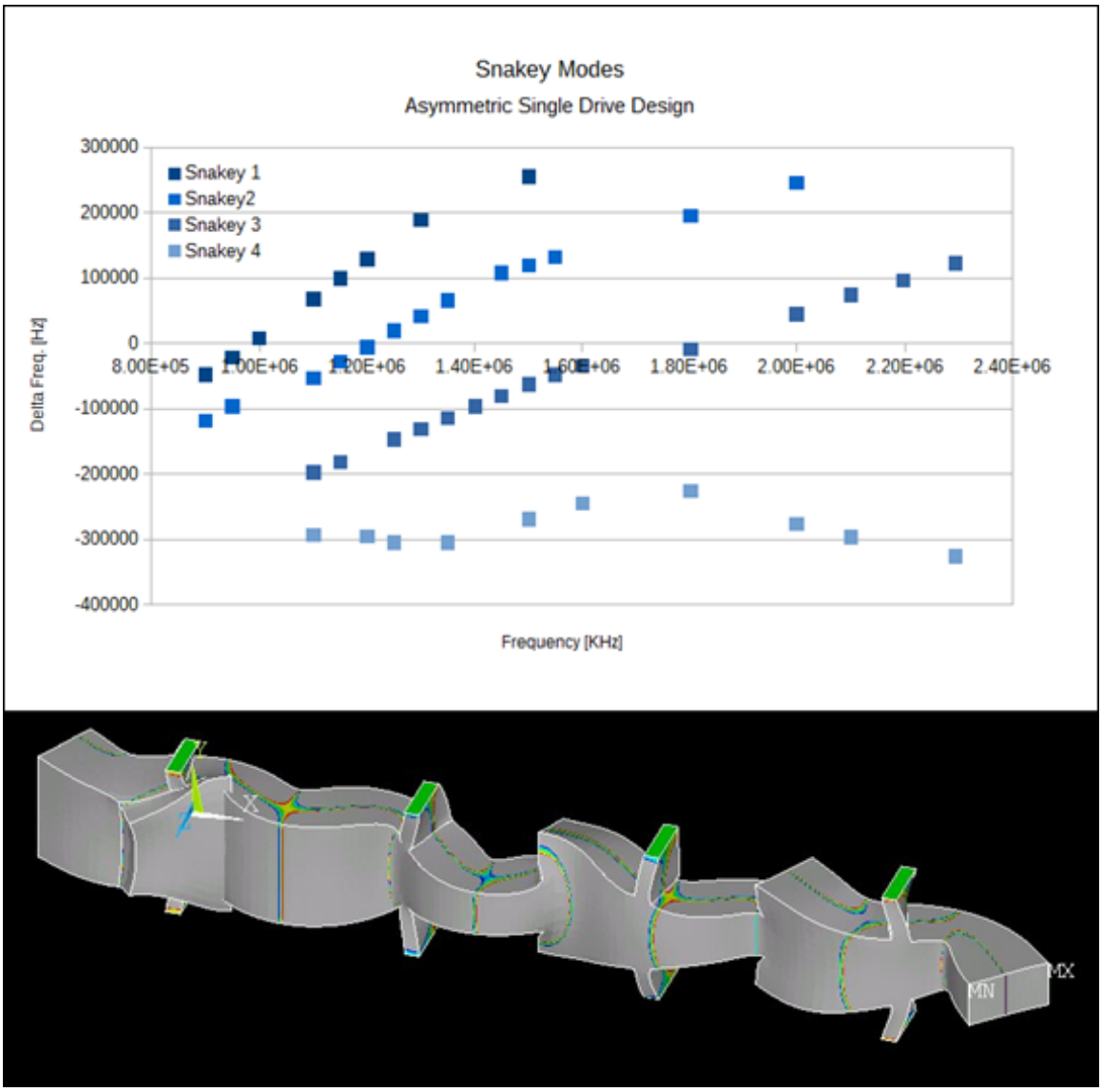

Figure 2.2: Snakey mode tracks and ANSYS X-Component of Displacement

for after beginning to extract the modal data of the ASD nozzle set. The snakey mode appears generally linear in nature with respect to the frequency with a slope of increase greater than unity. It intersects the longitudinal operation of the nozzle three times in the overall frequency range of my broad frequency study. The other mode tracks that I identified at this point can be found in Appendix B presented in the same fashion as the "snakey" mode in Figure 2.2. Next I will give a brief description of these various other modes that I found.

The "slightly hilly" mode, cataloged in Figure B.6 crosses the central mode at 1.5MHz. This lines up exactly with where the stress starts to transition into an exponential increase so this particular mode could possibly be a contributor to the the harmonic volatility seen in this region. Other than this, there are no other correlations observed which suggest that this mode has any effect on the ASD set at all.

The mode I initially labeled "pinch" was completely disregarded at first in its potential for being a source of the harmonic behavior in the central regime of the ASD set. The reason for this was due to the fact that the pinch mode track here had two very different regimes that were not associated with each other until the establishment of the 1.8MHz ASD nozzle. The 1.8MHz ASD nozzle simulation was one of the very last nozzle designs simulated for my research, well after most of the comparison studies had been completed. The first half of the pinch track is a gradual arc above the operational frequencies of the nozzle between 0.9MHz and 1.6MHz while it is found well below the operation of the nozzle by 2.0MHz. Once this connection was made, the proximity of this particular mode to the operation of the nozzle in the 1.6MHz-1.8MHz frequency range became very apparent. The second pinch mode intersects the longitudinal mode at 2.0MHz before moving well below the operation of the nozzle. The track plot and mode shape capture of this mode can be found in Figure B.7.

The snakey, slightly hilly, and the pinch are the modes with tracks that intersect the longitudinal mode of the nozzle in or around the central frequency regime where the harmonic spike is observed. Assuming the neighbor interference theory is the correct explanation of the spike, then any one of these modes or some combination of them is the cause of the harmonic spike. Thus, these three non-longitudinal neighbor mode tracks are plotted against the Z-normal stress in Figure 2.3. Recall that the ASD stress data plotted here is the same Z-normal stress data set that has already been featured in Figure 2.1.

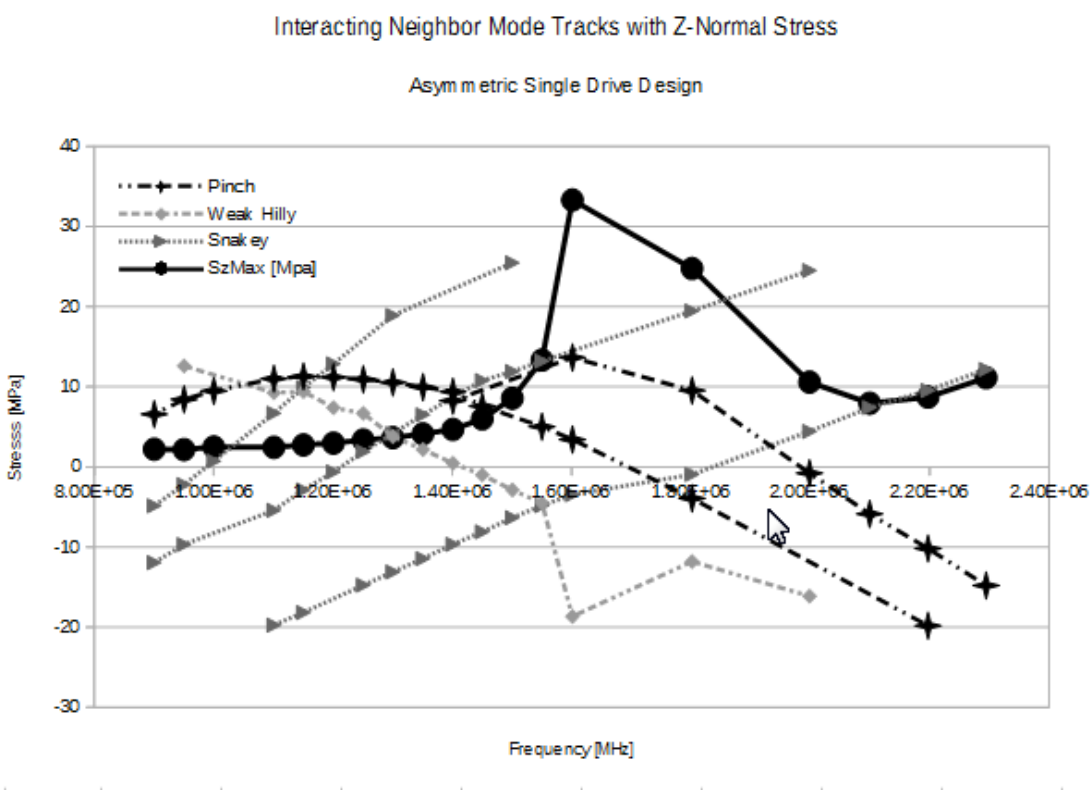

Figure 2.3: ASD Stress and Intersecting Mode Tracks

During this study there were a number of modes identified that appeared to be non-interacting for various reasons. These are the "corkscrewey" and "hilly" modes which can be found in Figure B.4 and Figure B.5 respectively. Two of the most prominent corkscrewey mode tracks have an inflection lining up with the center of the spike although they do not intersect it anywhere near that location. There are two intersections of this mode at 1.0MHz and 1.3MHz although no features of the nozzle's harmonic results were correlated with these crossings. The overall behavior of the corkscrewey modes is a mostly a gradual arc, rising in the 0.9MHz - 1.6MHz range and falling in the 2.0MHz - 2.3MHz range.

The hilly modes are even more unremarkable as they never seem to intersect the longitudinal mode at all. In fact, for the most part, they never even appear to deviate from tracking parallel to the operational mode of the nozzle. Because the

various tracks of the hilly mode keep nearly the same distance from the longitudinal mode of the nozzle over the entire frequency range, their effect on the nozzle will be the same for every nozzle in the ASD set. For this reason, no influence will be seen from this particular mode using the scaled comparison study method.

2.3 Linear Intersecting Interference

While building the initial ASD comparison set I had initially noticed that several of the modal tracks appeared to converge on the operation of the nozzle with the onset of the exponential increase in Z-normal stress. At this time I had only simulated ASD nozzles up to 1.6MHz. It appeared that the linear trajectory of the harmonic Z-normal stress transitioned into an exponential one just as this mode approached the operational frequency of the nozzle. However, the snakey mode had already been seen to intersect the operation of the nozzle at 1.0MHz and 1.2MHz with no discernible effect on the harmonic data of the nozzles.

I realized there could only two underlying causes for this behavior. Either the snakey mode had absolutely no effect on the harmonic results of the nozzle whatsoever and that its alignment here was a complete coincidence or, that this mode intersection was a necessary but not sufficient condition for the exponential increase in stress. The latter explanation required the snakey mode to interfere in conjunction with another non-longitudinal vibration mode or phenomenon that I had not yet seen any evidence for in order to cause the exponential increase in stress. In the chance that it was the latter case, I devised a hypothesis concerning the interaction between the nozzle operation and the snakey mode in the central frequency region. In order to begin to test it, a prediction was made about the behavior of the nozzles at frequencies above 1.6MHz that had not yet been simulated.

I postulated that the massive spike in nozzle stress, voltage, and power was actually a temporary phenomenon. If the third pass of the snakey mode was in fact a partial cause of the nozzle simulation data spike with its linear approach from beneath, then once it had passed the operational frequency of the nozzles of the ASD set and got far enough above it, the simulation data should return to the same linear increase that it had in the 0.9MHz-1.3MHz range. This was assuming that no other completely independent causes of nozzle operation degradation would come into play at these higher frequencies.

To find the location where I predicted that the harmonic results of the ASD nozzles would return to linear behavior, I first found the location where the nozzle harmonic stress of the ASD set started to deviate from a linear path and become exponential in its increase. As I have mentioned before, this occurs at around 1.4MHz. I took note of the width of separation between the "snakey" mode and the longitudinal mode at 1.4MHz for the corresponding scaled nozzle. Then, based on the linear slope of the snakey mode, I found the frequency when this same distance was once again seen between the snakey mode and the central mode: this time with the snakey mode above the longitudinal one. The frequency where this happened was roughly 2.1MHz. Here is where I proposed that the nozzle simulation parameters would return to their original linear behavior.

After finishing the higher frequency ADS nozzle designs I found exactly what I had hypothesized; the stress returned to the original linear relationship it had in the 0.9MHz-1.3MHz range. This proved that the spike in the harmonic results was a temporary phenomenon localized to the frequency range between 1.6MHz and 2.0MHz. While the center of the third snakey mode crossing was undoubtedly aligned with the center of the exponential stress spike, this did not actually show that the snakey mode was even partially responsible for it. In Figure 2.4 I re-plot the Z-normal stress

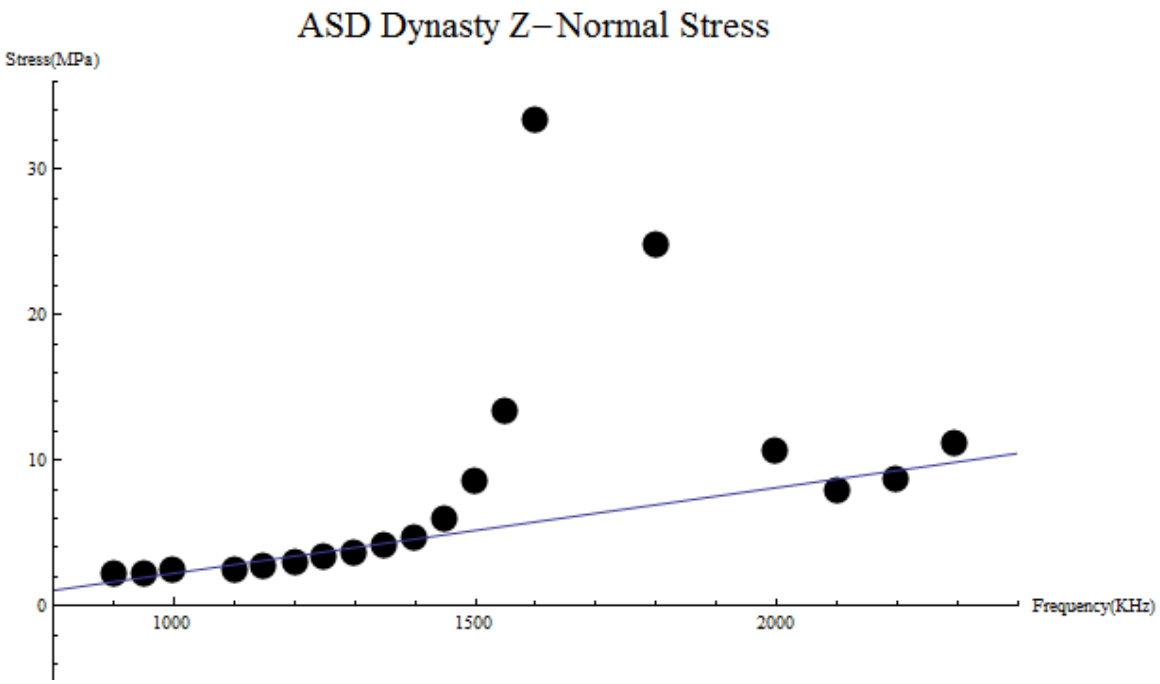

Figure 2.4: Asymmetric Single Drive Set Stress Linear Fit

of the ASD nozzle set partially fit to a linear equation. This is the same data set of stress from Figure 2.1 labeled as "ASD". Only the first 10 points of the data set are actually fit (0.9MHz - 1.4MHz) by the superimposed linear equation. Notice that the stress returns to its original linear path after reaching a peak at about 1.6MHz. This is the first demonstration that shows a non-longitudinal vibration focused within the piezoelectric element to be directly correlated with an increase in the harmonic stress.

2.4 Initial Nodal Support Position Study

This study is a basic comparison of the positions of the nodal supports of the entire ASD comparison set over its entire frequency range. During the ASD modal study I had first noticed that the locations of its position optimized modal supports seemed to move in the negative x-direction in a cyclic fashion. The final location of the nodal supports after the stress optimization process seemed to dip several times in

the negative x-direction towards the rear of the nozzle several times before returning to the neutral "zero" positions arbitrarily defined by the TrueGrid model mesh file. It was then noticed that this behavior seemed to line up with the intersections of the snakey mode and the operation of the nozzle.

To verify this initial observation, I compiled and plotted the final nodal bar positions against the operational frequency of all the members of the ASD set. I plotted where the x-dimension (longitudinal) location the nodal supports of each of these nozzles ended up after the position optimization process. This location was measured against the arbitrary nodal bar center as defined in the True Grid model file. The snakey mode results from Figure 2.2 are overlaid on the position of the driving support for the single drive nozzle. There is a clear correlation between the snakey mode tracks and the optimized positions of the support bars.

For clarity, I have split up the DSNS position data into two plots. The first, Figure 2.5, features the nodal support positions of the driving section and the first horn while Figure 2.6 does the same for the middle and tip horns. In each case, the position of these supports are plotted against the operational frequency of their nozzle, just like was done for all the earlier broad frequency studies featuring harmonic and modal data. Overlaid on both of the plots are the snakey mode tracks, clearly showing their intersection with the operational frequency.

Both of these plots clearly show a rearward shift in the stress optimized DSNS location lining up nearly perfectly with the intersection of the snakey modes with the central longitudinal mode. It is very clear that these snakey modes have a direct effect on the design of the nozzle individually and that there was a definite one-to-one relationship between them. That is to say that it does not appear that multiple neighbor modes working in conjunction are causing the dips, only the snakey modes. If another mode was necessary for this behavior to occur then I would have seen another mode in

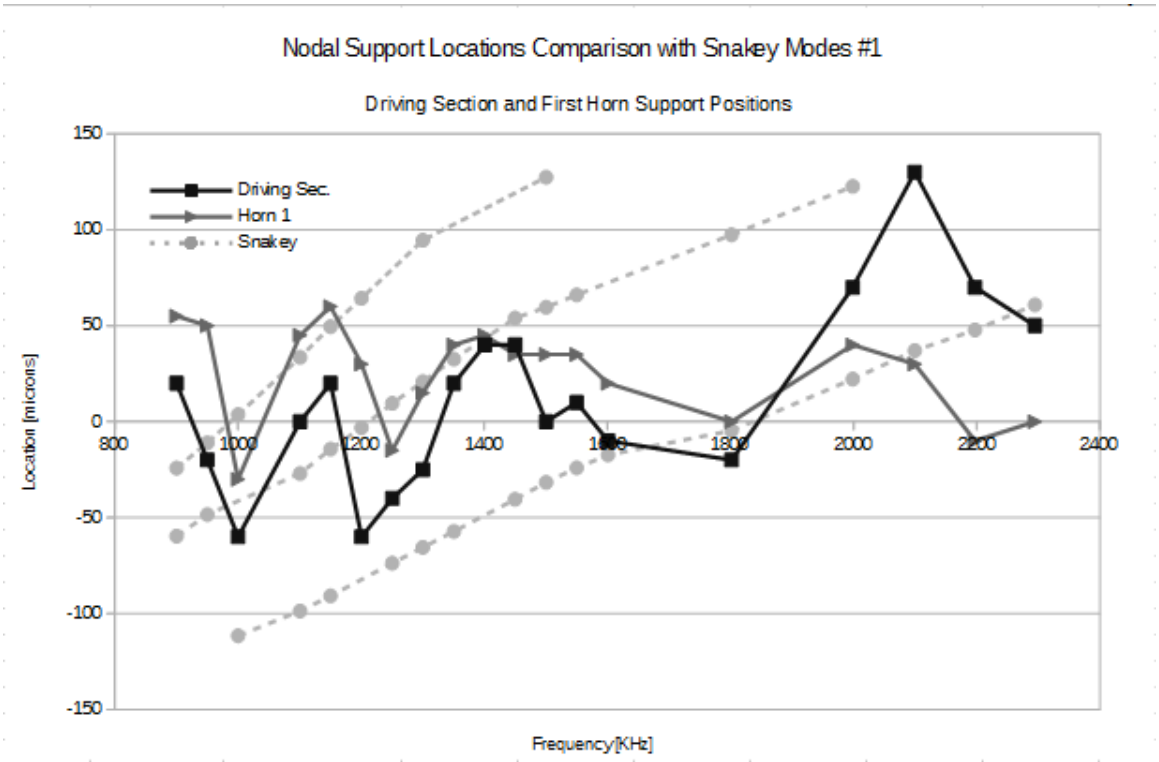

Figure 2.5: Driving Section and Horn Location vs. Neighbor Snakey Modes

the overall single drive mode plot Figure 2.3 appearing at all these locations just like the snakey mode which is not the case. Therefore, the multiple interacting mode hypothesis can be ruled. This phenomenon is likely closely related to the standing wave theory of the nozzles requiring the nodal supports to be placed 1/2 of the operational standing wave of the nozzle apart from each other. The theory behind this phenomenon is further in chapter 3.

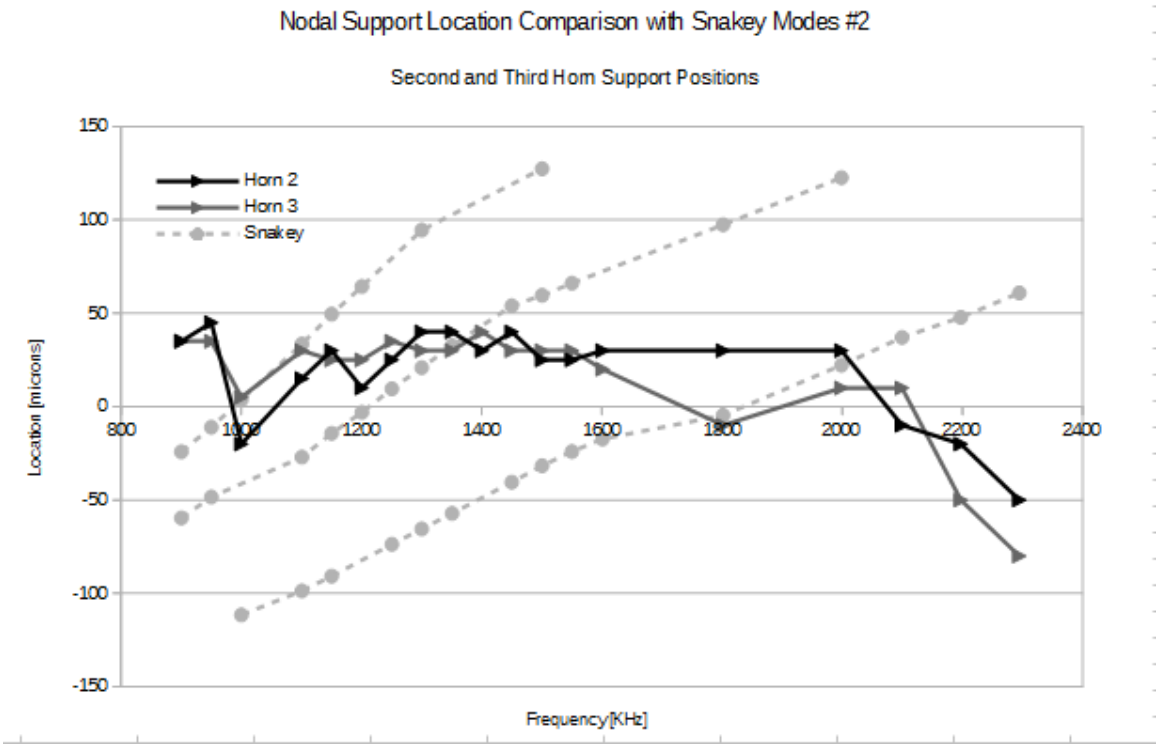

Figure 2.6: Horn 2 and Horn 3 Location vs. Neighbor Snakey Modes

2.5 Single Drive Thick DSNS Harmonic Results

In order to obtain the initial thick driving section support nozzle set , all that needed to be done was to thicken the driving supports of the original ASD nozzle design and carry out the nodal support optimization process. This thickness of 800 microns for the DSNS had been determined based on the DSNS thickness optimization of the 1.1MHz single drive nozzle. The stress data of this set is plotted in Figure 2.7 under the label "800μm ASD". The initial ASD stress data from Figure 2.1 is plotted as a control data set with the label "ASD" referring to the original thickness of the driving section nodal supports of the nozzle. The results for the voltage, power and impedance of the single drive nozzle studies discussed in this section are found in Figure C.8, Figure C.9 and Figure C.10 respectively.

From the Z-normal stress plot in Figure 2.7, the effect of thickening the driving section

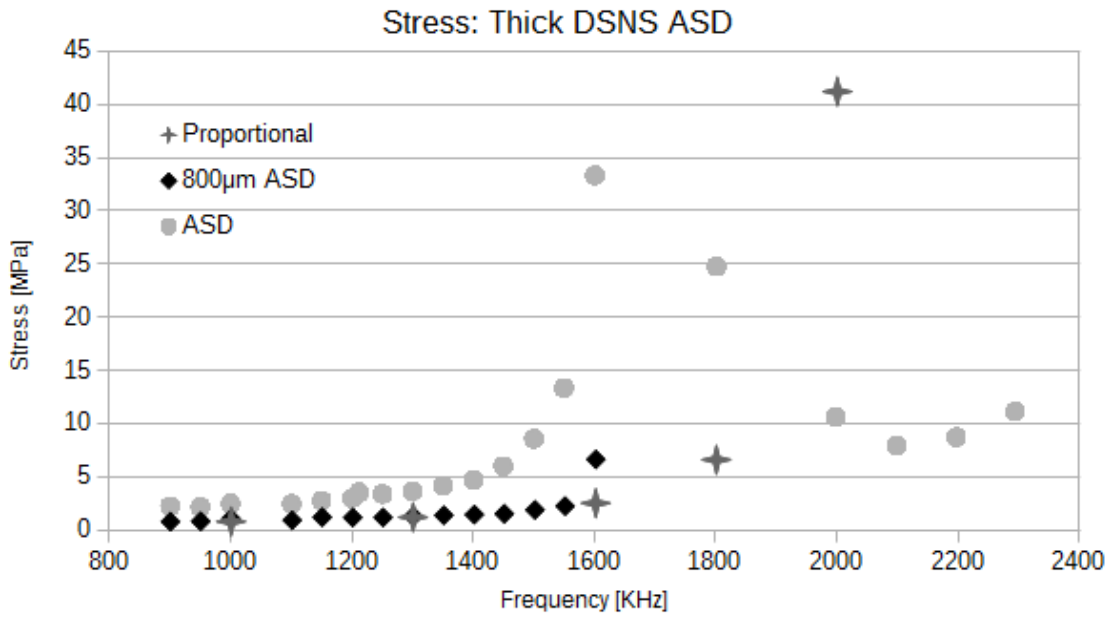

Figure 2.7: Single Drive DSNS Thickness Comparison

nodal support to a constant 800 microns initially appears to result in a significant improvement in the stress on the nozzle. While this improvement seems to be steadily increasing in its effectiveness with frequency compared to the 200μm ASD control data, it is sharply cut off at 1.6MHz where the nozzle quickly fails due to stress accumulation. The failure here appears in the form of a much quicker exponential increase which is only indicated by the sharp jump in the stress at 1.6MHz before the nozzle designs fail. All nozzles above this where either found to fail or were unable to be built at all due to the x-dimension width of the high frequency scaled transducer element becoming too small for the 800 micron thick DSNS supports.

In order to address this massive failure, the proportional thick DSNS nozzle modification was employed on a limited set of frequencies. Plotted in Figure 2.7 under the label "Proportional", this modification affected the trajectory of the ASD nozzle stress track much like the previous DSNS modification had done since the overall exponential increase remained. This time, however, the increase was made much more gradual than the original 200μm thick nozzle set. Beyond 2.0MHz, the proportional

thick design once again fails due to stress accumulation. The nozzles in the central 1.5MHz-1.8MHz range saw a significant improvement in stress over the original and 800 micron thick sets so this modification appears to have some utility in the central regime. The best explanation for the results of all three of these DSNS configurations is that they show the restriction of the nozzle operation by the by thick DSNS supports that are not kept small enough in proportion to the piezoelectric transducer for the higher frequency nozzle designs.

In general, the rest of the harmonic data plotted in Appendix C was also very interesting although not fully understood. The thick DSNS modification has a very strong effect on the voltage of the nozzle plotted in Figure C.8: completely eliminating the central voltage spike seen in the 200 and 800 micron thick DSNS sets. The harmonic voltage of the proportional set never exceeded about 8 volts before lining up again with the original ASD nozzle value again at 1.8MHz, something familiar from the ADS and ADD comparison in Figure 2.1 but not seen in the corresponding stress of this comparison.

The power of the proportional thick DSNS nozzle design in Figure C.9 follows the same exponential trajectory as seen in the stress. Also like the stress, the 800 micron thick DSNS show the sharpest increase while the proportional thick DSNS showed the most gradual. Finally it should be noted that the impedance data in Figure C.10 of all three different nozzle sets follow a very similar arcing trajectory in the lower half of the frequency range. In the upper half, however, each successive thick DSNS modification made in this section appears to progressively restore the impedance data to this original arc.

From these results it is clear that the thick driving section support increases the reliability of the ASD nozzles in the lower half of the overall frequency range. The initial modification of evenly thickening the DSNS to 800 microns does not seem to

really effect the underlying physical causes behind the harmonic value spikes except to cause it to shift slightly to a lower frequency. The proportional DSNS thickness nozzles it seems to affect this underlying cause of the exponential increase a bit more strongly but once again only shifting it a few hundred KHz higher. In short, the proportional thick DSNS method might have some limited utility in the lower frequency range but is not an improvement at all above about 1.5MHz. At this point the single drive thick DSNS nozzle set was abandoned in favor of exploring the dual drive version. However, the results of the initial thick DSNS were a great encouragement for me at this point to attempt to add more scaled nozzles to the "exponential" 1.6MHz -1.9MHz frequency regime which had previously been untenable due to catastrophic stress failure.

2.6 Dual Drive Thick DSNS Harmonic Results

The stress data of the original ADD nozzle along with that of its two modified DSNS thickness sets is presented in Figure 2.8. I found that for the 1.1MHz ADD design, the optimum stress value was given with both driving section supports set in unison to 600um. This thickness was then applied to all the nozzles of the original ADD set to create the constant thick DSNS ADD modification set. The harmonic Z-normal stress result from these nozzles are plotted in Figure 2.8 under the label "600μm". However, the thickness of the proportional DSNS plotted with the label "Proportional" is identical to the thickness of the single drive nozzle set featured in the single drive nozzle comparison. The original ADD dual drive set initially featured in Figure 2.1 is plotted as a comparison data set here with the label "ADD". The results for the voltage, power and impedance of the dual drive studies discussed in this section are found in Appendix D in Figure D.11, Figure D.12 and Figure D.13

respectively.

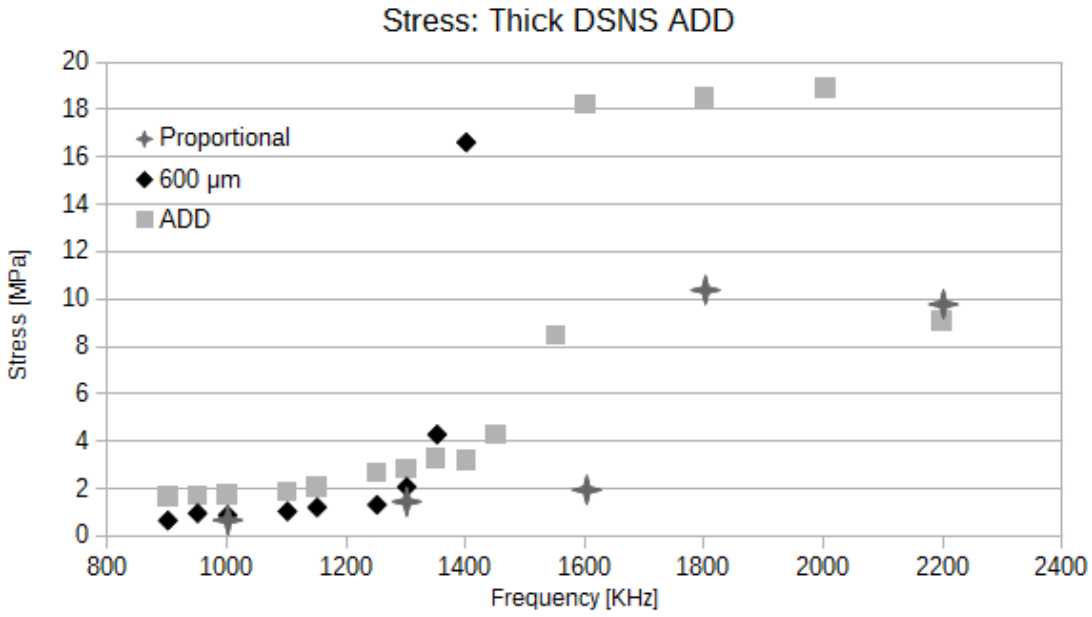

Figure 2.8: Dual Drive Thick DSNS: Stress

The improvement of the initial thick dual drive nozzles was much less effective overall in comparison to the improvement realized by the initial single drive modification. Even though this modification made a slight improvement in the nozzle performance in the frequency range from 0.9MHz to 1.3MHz, it was far less pronounced than the case for the single drive nozzle had initially been. Of far greater import however, is that it suffered an acute failure of the mode shape just after 1.3MHz. In fact, you can see in Figure 2.8 that by 1.35MHz, the stress of the thickened ADD nozzle had increased far beyond the original ADD value. This was also observed in the voltage and power data plots of Figure D.11 and Figure D.11 respectively. This result showed that the underlying cause of the harmonic data increase in the ADD nozzle set was more affected by the thickening process since the exponential increase was seen to shift forward significantly.

The proportional thick DSNS modification to the ADD nozzle showed much more promise by significantly improving the stress of the ADD nozzle in the 1.3MHz-

1.8MHz. In spite of cutting the stress of the dual drive nozzle to roughly half in this central frequency range, the proportional DSNS modification was unable to stop the ADD nozzle from exhibiting stress values far above the acceptable 4 MPa value. However, it was seen to converge back to the original ADD nozzle design at 2.2MHz.

Just like the stress, thickening the DSNS also lowers the voltage somewhat in the initial 0.9MHz to 1.6MHz frequency range. The double peak seen in the original ADD voltage data centered at 1.6MHz and 2.0MHz is completely erased by the implementation of the proportional thick DSNS. However, the proportional DSNS modification is unable to bring the voltage value down past the original ADD stress value at the 1.8MHz point for some unknown reason.

In terms of the power, it appears that thickening the DSNS proportionally eliminated the power spike seen at 1.6MHz although a steady increase in the power draw of the proportional thick DSNS nozzles is still seen overall, lining up once again with the original ADD nozzle at 2.2MHz. The power between the various designs follows the familiar pattern of matching closely in the 0.9MHz-1.3MHz and the 2.0MHz+ frequency ranges but diverging from each other in the central range.

The impedance of all of the various ADD DSNS designs plotted here is much flatter compared to the previous thick DSNS ASD and ADD set plotted in Figure C.10 and Figure A.3. Besides the same outlier data point in the original ADD data set, the impedance between the various thick DSNS nozzles does not vary significantly with frequency.

Once again we see that at the 2.2MHz frequency point all of the harmonic nozzle values converge on each other after becoming highly separated in the central frequency region from about 1.3MHz - 2.0MHz. This was not something that was seen in the ASD nozzle set due to the failure of the ASD nozzle above 2.0MHz. However, this was

the pattern seen earlier in the 0.9MHz-1.3MHz frequency range where in the initial ASD vs. ADD stress plot.

In spite of the clear improvement seen by the proportional thick DSNS to the dual drive nozzle in the central region, another modification will be needed to get these nozzle designs into an acceptable range for potential fabrication, especially those at higher frequencies.

2.7 Advanced DSNS Modification Study

The effects that a series of cumulative nozzle modifications have on the relationship between the non-longitudinal neighbor modes and the harmonic simulation results will be explored in this section. All of the modifications featured in this study are arranged in order of increasing effectiveness in improving the harmonic simulation results. Each modified nozzle set is used as the control set for the next modification with the initial control being the ADS set. The modifications featured here are that of adding a second driving section, optimizing the DSNS of the ADD nozzle by their thickness and then lastly optimizing all the nodal supports by their position.

The Z-normal stress progression of all the nozzle modification sets featured in this study is plotted in Figure 2.9. This plot tracks the continual improvement of the harmonic data due to sequence of modifications taking the initial ASD nozzles to the final thickness and position optimized DSNS ADD nozzle designs. The initial control group and the first modification data sets are identical to the ASD and ADD sets first plotted in Figure 2.1. They are labeled here as “ASD” and “ADD” respectively. The two new nozzle sets featured here are the dual DSNS thickness optimized nozzle set labeled “DOT” and its DSNS position optimized progeny labeled “PDOT”. The

rest of the harmonic data is plotted in a similar fashion in Appendix E.

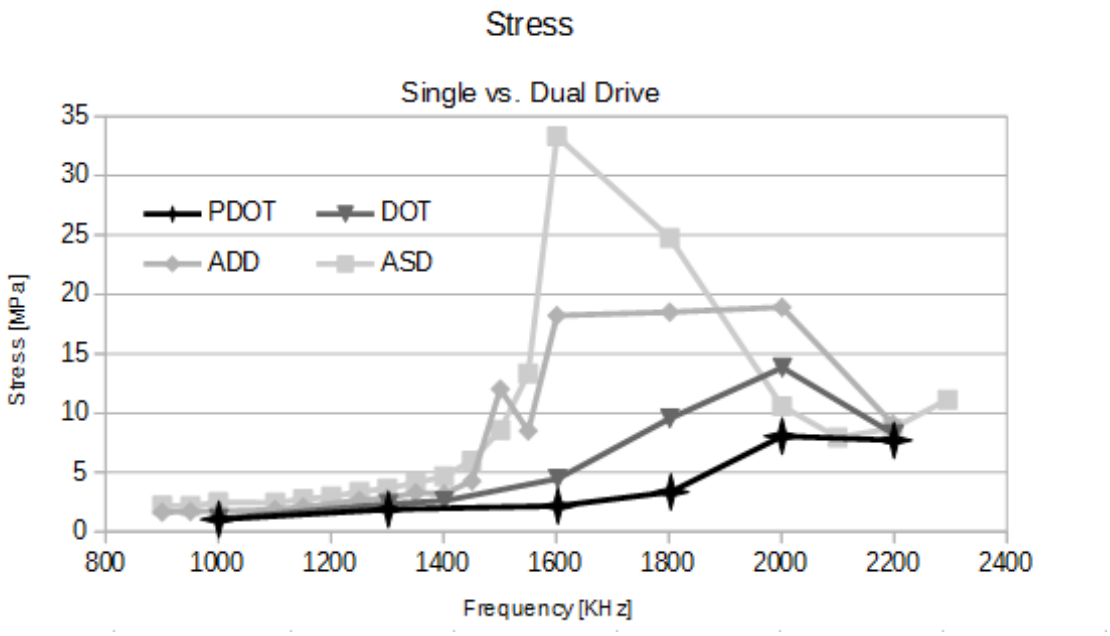

Figure 2.9: Modification Harmonic Comparisons: Stress

In the Z-normal stress comparison plot, the overall range of improvement made to the nozzle by the featured modifications can be clearly seen. Much like was seen in earlier simulation comparisons the modifications essentially make no impact on the stress results of the nozzles within the linear regime of the broad frequency range while making a significant improvement to those in the spike regime. Overall, the sequence of modifications worked in conjunction to bring the stress down to fully acceptable levels below 1.8MHz. The modifications also made little difference in the post-spike regime as all the stress data converges, once again matching a pattern seen in many of the earlier simulation comparisons.

In spite of the outstanding performance of the nozzle modifications in the spike regime, the original "linear" stress increase is still seen holding over the whole range. Above 1.8MHz, even the stress of the highest performing "PDOT" nozzle designs clearly surpasses the upper threshold of acceptable nozzle operation. The stress seems to level off at about 8MPa above 2.0MHz for all the designs until the end of the data

set at 2.2MHz and 2.3MHz. The general trends seen in these stress results are also mirrored in the voltage and power data sets in Figure E.14 and Figure E.15. The impedance featured in Figure E.16 also shows a familiar path.

The second major part of this study is exploring the effect that each of these nozzle modifications have on select non-longitudinal mode tracks. Specifically that of the "snakey" and the "pinch" mode classes. Each of these plots is a comparison of the same set of mode tracks of a nozzle before and after it is modified. The control set in each case is the previously modified nozzle set. In each plot, the control mode tracks are plotted in a lighter color featuring dashed connecting lines while the modified data is darker with solid lines.

The pinch mode tracks for each successive modification are found in Figure 2.10. The pinch modes were chosen for exposition here once it was realized that it was the most likely candidate for the harmonic spike. The corresponding snakey mode track plots can be found in Appendix F. It is very interesting to note that the snakey mode had almost no interaction with the various modifications to the nozzles. This result, while not surprising in and of itself, offers a good contrast the the behavior of the pinch mode.

The first striking feature of these plots is the difference between the pinch modes of the single drive and dual drive nozzles in Figure 2.10a. While there were only two major pinch modes present in the ASD set, adding the second drive results in four major modes of this type that can be tracked over much of the frequency range.

The next nozzle modification of adjusting the thickness of the DSNS of the ADD set to its optimized value is plotted under the label "DOT" for "Dual Optimized Thickness". The mode track shifts due to this modification is plotted in Figure 2.10b has an even more significant effect on the pinch mode tracks. Here it is very clear

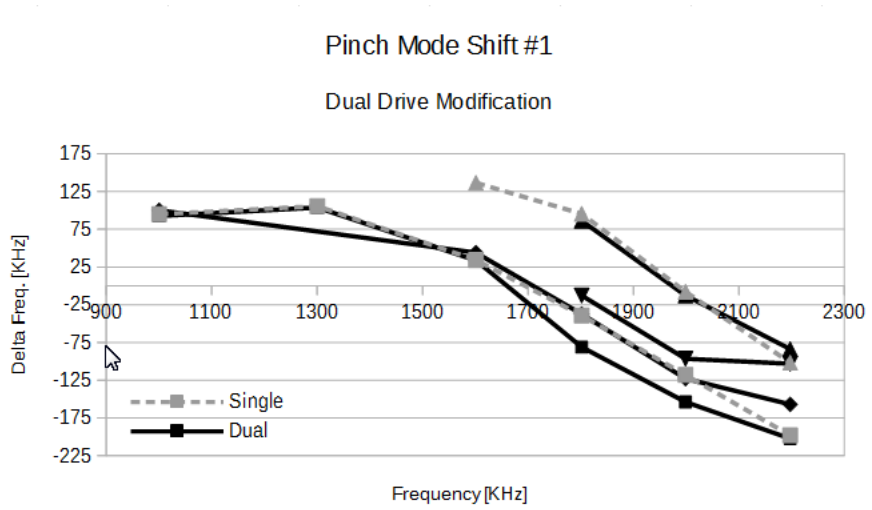

(a) Dual Drive Modification Pinch Mode Shift

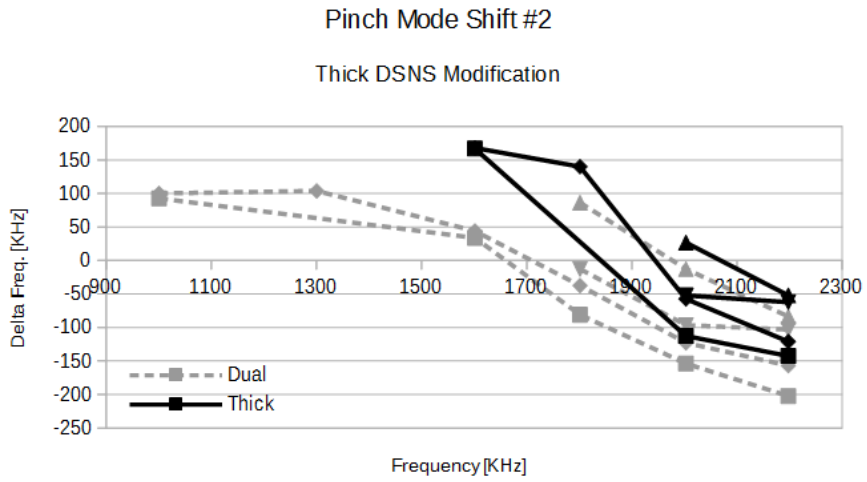

(b) Thick DSNS Modification Pinch Mode Shift

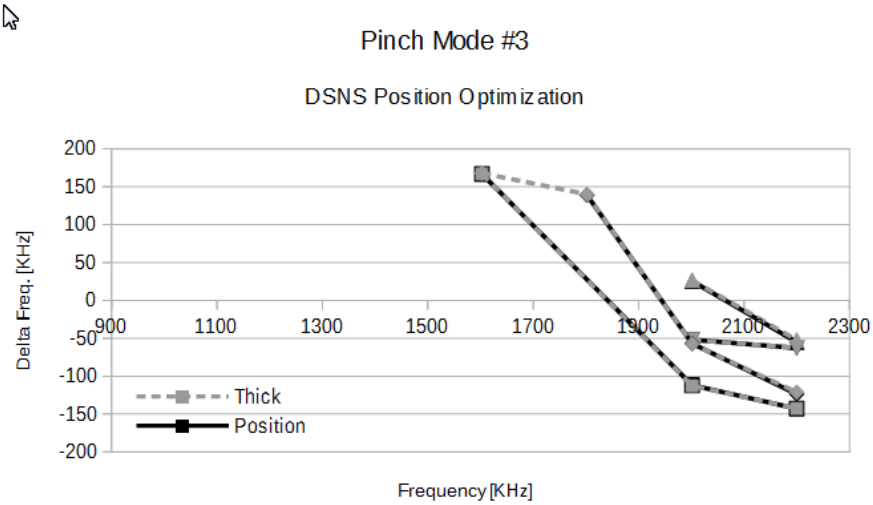

(c) Position Optimization Modification Pinch Mode Shift

Figure 2.10: Pinch Mode Shifts Resulting from Nozzle Modifications

that thickening the DSNS causes the intersection of the pinch mode to shift higher in frequency and become steeper. Unlike the pinch mode track response to the previous "ADD" modification of adding a second drive, the number of major pinch mode tracks here does not change.

Lastly, it is clear from Figure 2.10c that the effect of optimizing the DSNS by their position clearly has no effect on any of the piezo pinch mode tracks. I have labeled this modification as "PDOT" for "Position Dual Optimized Stress". All of the pinch mode tracks remain bunched up above 1.8MHz exactly where they were left by the "DOT" modification. This finding is especially interesting when contrasted with the PDOT harmonic results in Figure 2.9 where an improvement in the Z-normal stress from the "PDOT" modification was seen to be equal to that of the "DOT" of the DSNS thickening modification which caused a significant shift in the pinch mode tracks.

It is interesting to note that while every modification featured in this study results in roughly the same contribution to the improvement of the Z-normal stress. However, the effect on the on the non-longitudinal neighbor modes is clearly not as consistent. In fact, it can be seen in Figure F.17, that none of the featured nozzle modifications have any major effect on the snakey mode tracks.

Of these three nozzle modifications, it is very obvious that only one of them has a direct effect on a previously defined non-longitudinal mode track: the effect of the "POT" on the pinch mode. The only other major mode track effect seen here is the addition of several tracks with the second driving section in the "ADD" modification.

The modification comparison plots of the modal data show that it is possible to improve the harmonic results of a nozzle design in two separate ways: both with and without a corresponding shift in the non-longitudinal neighbor mode tracks. This

shows that there is another fundamental mechanism which can effect the harmonic results of the nozzle with no direct interference from a piezoelectric element focused non-longitudinal neighbor mode.

2.8 Symmetric Nozzle Comparison

This limited comparison study takes an overarching selection of nozzle simulation designs that I have developed throughout the course of my research and compares them at the two paramount frequencies of 1.0MHz and 2.0MHz. The designs featured in this comparison are the ADS, ADD, DSNS optimized ADD nozzle, and lastly the symmetric dual drive (SDD). The data is presented in tables. The ANSYS harmonic simulation results for the 1.0MHz nozzles are given in Table 2.1 while that of each of their 2.0MHz counterparts can be found in Table 2.2. The asterisk signifies that there are multiple versions of the listed design ID. The newest version is utilized here. A comparison of the modal data at 1.6MHz would offer an even more resolved understanding of the differences between the various versions of the nozzle and would be a good comparison to add to this in the future.

Table 2.1: Nozzle Comparison at 1.0 MHz

Config.	Design ID	Freq [KHz]	V App. [V]	StressZ [Mpa]	Pwr [mW]
ASD	M10NCH568*	1000.35	6.976	2.49	19.82
ADD	M10NCH572*	1000.35	3.854	1.74	21.67
PDOT	M10NCH600	1000.92	2.974	1.05	20.97
SDD	M10NCH581	1001.02	2.652	0.59	21.01

The 1.0MHz nozzle results in Table 2.1 show a continual improvement in Z-normal stress following the natural progression of nozzle modifications established in the DSNS modification study. The 1.0MHz SDD design exhibited the most superior

performance with a Z-normal stress of almost half that of the next best design. This same trend is also mirrored in the minimum voltages required to run the nozzles. The power requirement, however, is lower for the ASD and the optimum thick ADD designs while it is higher for the original ADD and the dual symmetric.

Table 2.2: Nozzle Comparison at 2.0 MHz

Config.	Design ID	Freq [KHz]	V App. [V]	StressZ [Mpa]	Pwr [mW]
ASD	M20NCH529	1998.72	3.203	10.59	17.86
ADD	M20NCH545	2002.78	13.22	18.93	52.01
PDOT	M20NCH549	2000.93	1.417	8.06	18.18
SDD	M20NCH560	2001.48	2.95	20.49	39.18

The various nozzle designs at 2.0MHz, however, do not follow this pattern at all. Initially it was seen that that at this higher frequency, adding the second drive to the original ASD nozzle design without thickening the DSNS actually makes the Z-normal stress result significantly worse. In fact, for the dual symmetric design, the Z-normal stress was double that of the original ADS design with the ADD design it was not much better. The only improvement at 2.0MHz is done by thickening the DSNS supports as was done for the ADD model here even though it Z-normal stress is almost 3 times as large as the worst 1.0MHz nozzle (ADS).

The vast majority of the nozzles have a power requirement of around 20 [mW] with two significant exceptions: the 2.0MHz dual symmetric and ADD drive designs. It is very interesting to note that in light of this, the 2.0MHz ADD optimum thick DSNS and the ADS design have power requirements right in line with the rest of the 1.0MHz nozzles. It is almost as if this threshold of 20 [mW] is the minimum power requirement of the nozzle regardless of the driving section configuration provided that the nozzle has been optimized sufficiently. Of these two designs there is also a major discrepancy in their minimum voltage: the 2.0MHz symmetric nozzle design has a minimum voltage that is in the range of most of the other nozzles while the original

ADD voltage requirement is roughly 3 times larger. Lastly, for both the 1.0MHz and 2.0MHz cases, every type of dual drive nozzle design always requires more power than the ASD design, although in many cases this difference was negligible.

The modal data, presented in fig. 2.11, is a collection of individual tables each closely resembling the ANSYS modal analysis "read results by pick" table. This table lists all of the frequencies of the various non-longitudinal modes found in each nozzle design centered around the operational "longitudinal" mode. Recall that it is from this table that I calculate each of the "Delta Frequency" data points that make up the non-longitudinal mode track plots. The frequency tables of each of these 8 nozzles are presented here with one important modification: their frequencies are binary coded by their overall vibration shape.

The top half of fig. 2.11 contains the mode frequencies of the nozzle designs operating at 1.0MHz while the bottom half are those at 2.0MHz. The columns are the designs of ADS, ADD, Optimum thick ADD, and SDD in order from left to right. The key aspect of this plot is the binary color coding. All of the frequencies in the table that represent horn-centric modes are coded with a white background while the piezo-centric modes are given a black background.

Each individual horn-centric non-longitudinal mode shape is given a unique nozzle identification number which is keyed in fig. 2.12. This was not done for the piezo-centric modes. Instead they are all identified with a single number matching that of the pinch mode first found to operate within the ASD set. The piezo-modes afflicting the 2.0MHz nozzle design had so many unique yet similar shapes that it was impractical to try to resolve all of them. Since these modes only began to appear in the modal results of the highest frequency members of the ASD set, their mode tracks would not be enlightening. In fig. 2.13 the screen shots of various piezo-centric mode shapes found in the 2.0MHz ADD nozzle are displayed, almost all of these modes

1.0MHz ASD	ID #
8.43032E+05	5
8.62971E+05	6
9.03547E+05	4
9.14199E+05	5
9.31409E+05	7
9.95465E+05	2
1.00035E+06	**1**
1.00769E+06	4
1.03807E+06	7
1.07707E+06	6
1.09526E+06	3
1.10101E+06	6
1.12640E+06	8
1.16039E+06	4
1.18402E+06	4

1.0MHz ADD	ID #
8.34553E+05	4
8.64802E+05	6
9.10591E+05	5
9.20534E+05	6
9.35123E+05	4
9.57268E+05	2
9.95459E+05	2
1.00035E+06	**1**
1.01224E+06	4
1.03274E+06	5
1.06632E+06	5
1.07563E+06	6
1.09302E+06	3
1.10041E+06	3
1.10718E+06	6

1.0MHz T.ADD	ID #
8.04912E+05	3
8.08020E+05	9
8.48367E+05	4
8.68387E+05	6
8.84338E+05	7
9.24395E+05	5
9.48132E+05	4
9.57272E+05	**1**
1.00092E+06	1
1.01904E+06	4
1.02668E+06	7
1.03904E+06	5
1.05897E+06	8
1.08263E+06	6
1.11904E+06	4

1.0MHz SDD	ID #
7.65640E+05	4
8.36784E+05	5
8.44856E+05	6
8.87225E+05	6
8.94562E+05	4
9.19724E+05	5
9.65916E+05	2
1.00102E+06	**1**
1.00417E+06	4
1.00735E+06	4
1.01670E+06	8
1.03256E+06	5
1.07582E+06	6
1.09673E+06	5
1.15196E+06	4

2.0MHz ASD	ID #
1.72161E+06	4
1.73600E+06	5
1.88067E+06	8
1.88835E+06	5
1.93572E+06	2
1.99093E+06	3
1.99866E+06	**1**
2.03118E+06	5
2.04304E+06	4
2.04391E+06	2
2.13950E+06	5
2.24076E+06	7
2.24382E+06	4
2.30059E+06	3
2.33127E+06	8

2.0MHz ADD	ID #
1.84894E+06	3
1.87986E+06	11
1.89852E+06	5
1.90625E+06	8
1.94083E+06	7
1.99090E+06	3
1.99392E+06	3
2.00278E+06	3
2.01849E+06	8
2.04459E+06	2
2.05169E+06	4
2.13278E+06	5
2.22063E+06	4
2.22601E+06	7
2.28831E+06	4

2.0MHz T.ADD	ID #
1.80385E+06	8
1.86997E+06	8
1.88905E+06	3
1.91985E+06	7
1.94407E+06	3
1.94907E+06	3
1.94977E+06	2
2.00093E+06	**1**
2.02651E+06	3
2.04055E+06	3
2.04149E+06	2
2.05566E+06	4
2.11174E+06	7
2.14550E+06	5
2.22230E+06	4

2.0MHz SDD	ID #
1.79039E+06	8
1.85202E+06	3
1.86579E+06	3
1.89123E+06	5
1.90333E+06	6
1.90837E+06	3
1.97997E+06	3
2.00148E+06	**1**
2.03628E+06	3
2.04833E+06	5
2.06816E+06	3
2.10412E+06	4
2.17199E+06	3
2.17500E+06	5
2.18187E+06	7

Figure 2.11: Vibration Mode Shape Comparison

shape classes have counterparts in the other 2.0MHz nozzle designs.

Comparing the nozzle designs of each paramount frequency by their harmonic results, it was clear that the 1.0MHz nozzles possess markedly superior performance. For every nozzle design, the 1.0MHz version was superior to its 2.0MHz counterpart. This discrepancy was especially pronounced in the symmetric nozzle design although it was very strong in the asymmetric nozzle designs as well. A comparison of the modal results offered an immediate explanation for this: the significant encroachment of piezo-modes on the frequency of the nozzle. This finding is consistent with the pinch

1	Longitudinal
2	Corkscrewey
3	Pinch + Piezo-centric
4	Snakey
5	Hilly
6	Propeller
7	Mixed hilly
8	Slightly Hilly

Figure 2.12: Vibration Mode Shape Comparison Key

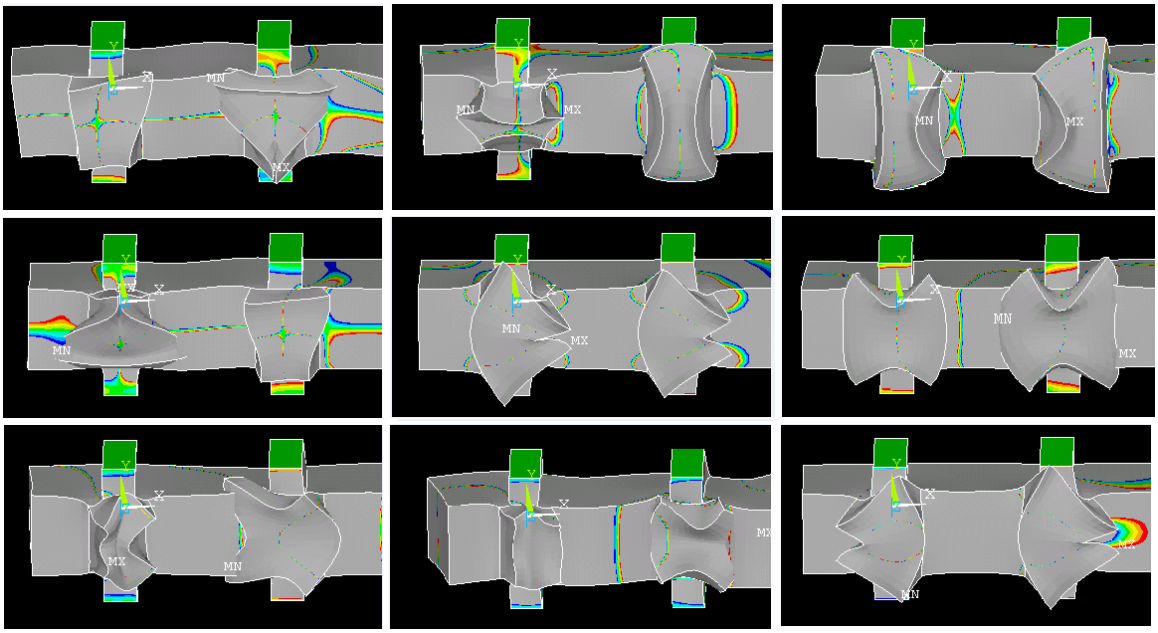

Figure 2.13: 2.0MHz ADD Nozzle Piezoelectric Element Centric Modes

modes being shown to intersect the operation of the ASD nozzles at the center of the stress spike.

The purpose of presenting the non-longitudinal neighbor mode data in fig. 2.11 is to simply show the overwhelming influx of black labeled piezo-modes in the 2.0MHz designs. Even though for the 2.0MHZ ASD nozzle only two were seen, the were right on top of the operation of the nozzle, something clearly not observed in any of the 1.0MHz nozzle designs. For the the 2.0MHz ADD, the piezo-modes were so close to the operation of the nozzle that they completely overpowered the longitudinal mode

hindering it from being resolved by the modal analysis simulation. Based on these results, I speculated here these various piezo-modes had been steadily approaching on the operation of the nozzle slowly over the entire comparison set and that this appears to the cause of the underlying "linear" increase of the nozzle Z-normal stress seen over the entire broad frequency range. Therefore, the underlying cause of the harmonic stress spike and the underlying linear increase can now be seen to have the exact same underlying cause: destructive interference from vibrations focused in the piezoelectric transducer plate.

2.9 Nozzle Symmetry Comparison

I will now address the discrepancy in performance seen between the asymmetric and symmetric nozzle designs, specifically those of the ADD and SDD. At any given frequency, these two designs posses identical piezoelectric elements and horn dimensions; only the number of driving sections and the bonding configuration of piezoelectric elements will differ. While this comparison is only of the 1.0MHz nozzles in table 2.1, any general information concerning their relative performance obtained from them will be assumed to be applicable to symmetric and asymmetric nozzles of any frequency.

Shown in fig. 2.14 is a visual comparison of the standing wave nodes of the longitudinal vibration of the 1.0MHz ADD and SDD nozzle driving sections. In both cases, the nozzles are pointing to the left. In the former case, only the second driving section is shown. Here, only the smallest absolute amplitude magnitude of the longitudinal x-dimension of displacement is shown. Therefore, the contour lines of these plots trace the nodes of the longitudinal standing wave.

The x-displacement contour node on the back of the ADD driving section is not

centered on the support but rather is displaced towards the front of the nozzle. This exact same phenomenon is also seen in the driving section of the ASD nozzle (not pictured). In contrast, for the symmetric SDD nozzle driving section shown on the left, it is clear that this wave is supported equally on each side resulting in a wave that propagates along the nozzle x-axis in a centered fashion.

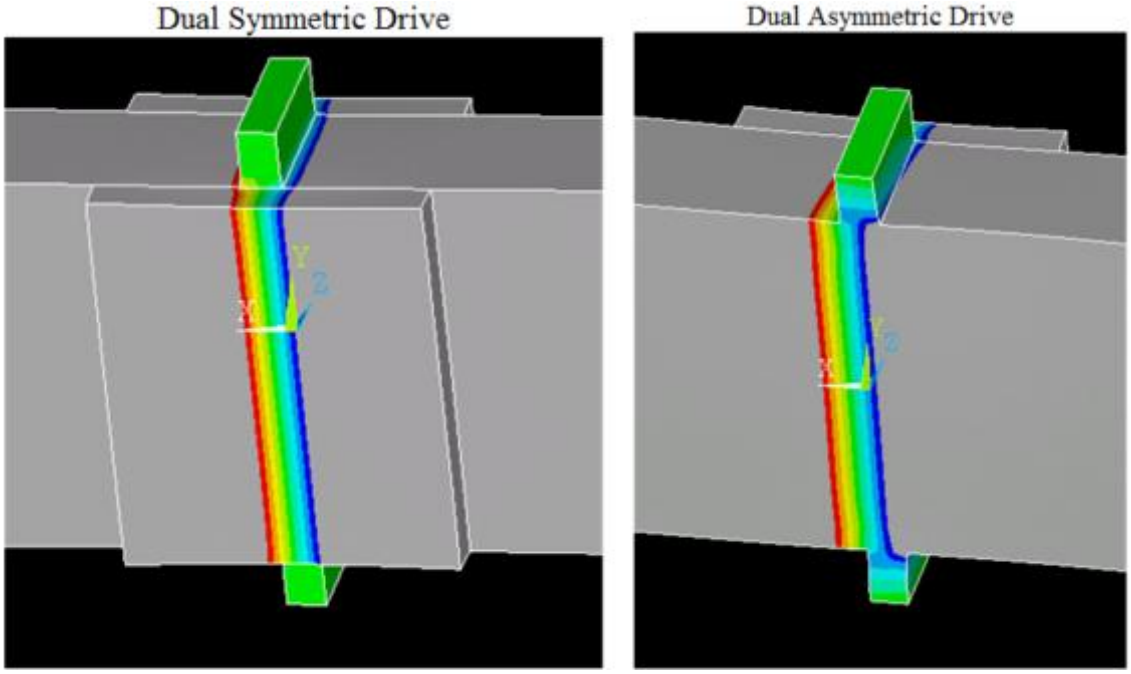

Figure 2.14: Dual Symmetric vs. Asymmetric Tip Node Compare

This misaligned mode phenomenon seen in the ADD driving section only becomes more acute for its horn nodes. In fig. 2.15 a screen shot of the backside (opposite side from piezoelectric elements) of the tip horn of the 1.0MHz ADD nozzle is compared with the tip horn of the symmetric SDD case. It is very clear the standing wave nodes are not lining up with the longitudinal axis of the ADD nozzle meaning that the longitudinal vibrations are not propagating completely straight down the nozzle. The symmetric nozzle in comparison, still has very straight nodes even at its tip horn where there is no perceptible displacement between the nodes and the support bars on either side of the nozzle.

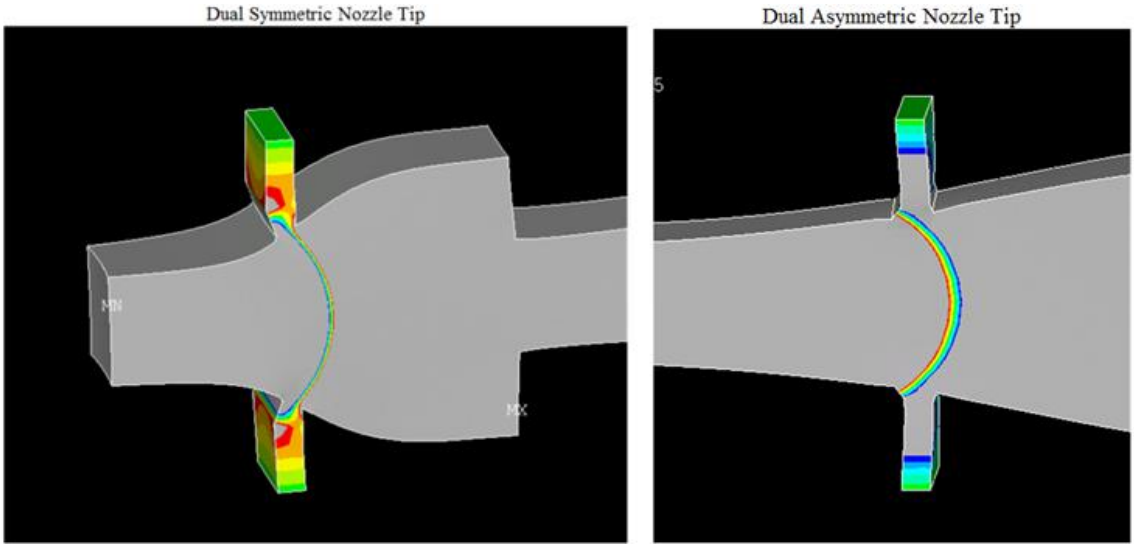

Figure 2.15: Dual Symmetric vs. Asymmetric Tip Node Compare

Based on these results, it is clear that the displacement of the standing wave set up by the ADD nozzle is not resolving to be completely normal to the longitudinal axis of the nozzle as it was originally designed. I propose that this misalignment is the source of the discrepancy seen between the harmonic results of the 1.0MHz ADD and SDD harmonic nozzle results seen in table 2.1. The vibration input asymmetric nozzle is fundamentally unbalanced since the piezoelectric elements only introduce the vibrations on one side of the silicon nozzle body. This uneven forcing introduces more stress into the nozzle's operation causing it to be less reliable and require greater power and voltage for the transfer of vibrations.

The unbalanced nature of the vibrations is likely to result in much more robust non-longitudinal modes displacing the nozzle more readily outside of the x-y plane vastly increasing the z-normal stress. This increased stress will cause the nozzle operation to degrade faster than it would for the more balanced symmetrical case as the bonding integrity will be adversely affected.

Although the stress of the 1.0MHz ADD nozzle is almost three times higher than the 1.0MHz SDD nozzle it still features acceptable harmonic results. The optimum thick

DSNS modification brings this value down to under twice the SDD stress amount. From this it is clear that although the asymmetric design is inferior to a directly comparable symmetric design, it still offers excellent performance provided it is not afflicted by destructive interference. For this reason it is clear that future research devoted to improving the nozzle of all designs should be focused on addressing the destructive interference inherent in the piezoelectric transducer plates at higher frequencies. This will be the most effective action for improvement of future nozzle designs, especially those intended to operate at higher frequencies.

Chapter 3

Conclusion

I will conclude by giving an overview of all the separate underlying mechanisms by which the nozzle's performance is seen to be affected. This will be done to build a framework of understanding that can later be employed to direct the design of more advanced nozzles at any frequency. Based the results of all the simulation studies, I have found that there are several different fundamental causes behind affecting the behavior of the nozzle.

By far the strongest effect, and the only one that was seen to affect the harmonic results directly, was the vibration mode limited to the piezoelectric element known at the piezo-mode. Vibrations of this sort were shown to directly correlate to two separate components of the harmonic stress increase. The first was a linear intersection of the single "pinch" mode class which directly lined up with the central harmonic spike. The second was the steady linear stress increase attributed to the constant approach of multiple piezo-modes which manifested in every nozzle design operating at 2.0MHz.

Physically, the spatial domain of the piezo-mode offers a very straightforward ex-

planation for the observed increase in stress. This type of vibration mode results in a focused distortion of the piezoelectric element that is unable to translate into a longitudinal standing wave in the nozzle body. Because of this mismatch, there is a massive build up in stress at the bonding interface whenever this mode type of mode becomes activated. It is exactly at this interface where the harmonic Z-normal stress is taken by the simulation. The strength of the bond between the piezoelectric element and the silicon crystal wafer offers the best measurement of the longevity of the nozzle since during normal operation of the nozzle, this is overwhelmingly the most likely point of mechanical failure.

Not as obvious is the fact that a vibrational distortion spread evenly over the entire nozzle was shown to have no effect on the harmonic results of the nozzle even when it directly interfered with the standing wave of the nozzle. This was seen in the direct correlation between the "snakey" horn mode with the final optimized locations of the nozzle support bars. Whether this particular type of interference has a direct effect on creation of a monodisperse aerosol via the temporal Faraday wave instability at the nozzle end face is outside the scope of this research and will need to be tested experimentally.

While evidence supporting the non-longitudinal mode interference hypothesis has been demonstrated in multiple ways, it was also very clear that the nozzle's stress performance could be greatly affected in a manner that did not involve interference from an non-longitudinal mode at all. It was demonstrated in the advanced DSNS modification study that the stress of the un-optimized DOT nozzle design was greatly improved by adjusting the locations of the nodal supports with no corresponding change in the snakey or the pinch modes. This was in spite of the fact that the optimum positioning of the supports of the nozzle clearly correlated with the intersection of the snakey horn mode. This means that while the snakey mode in the nozzle body

directly interfered with the longitudinal standing wave of the nozzle by shifting its nodes, it had absolutely no effect on the harmonic results in doing so, especially the Z-normal stress.

The improvement that was made in the DSNS modification by optimizing the support positions was roughly equivalent to the DSNS thickness modification that was seen to directly suppress the pinch mode. The position optimization process appears to fully address the suppression of the longitudinal vibration so this effect is not considered to an issue that needs to be addressed further. However, there was direct proof that a non-longitudinal mode could directly interfere with this standing wave which confirms that the longitudinal mode takes the form of a standing wave in the nozzle. It offers a relevant comparison to the improvement to the nozzle made by directly suppressing a piezoelectric vibration intersecting the nozzle operation.

The thick DSNS modification has proved to be very effective when addressing the effect of the piezoelectric pinch mode in the central frequency region where it directly intersected the operation of the nozzle. When the modal results are viewed it is very clear that this modification is directly suppressing the distortion of the "pinch" piezo-mode. It might do this by directing more vibration at that frequency to into the nozzle body resulting in a more robust standing wave. While allowing the width of the DSNS to get larger may in fact be suppressing the standing wave around its nodes, compared to the overall improvement of the nozzle close to the pinch mode intersection, this degradation is negligible. Overall, these results show that in regions where the piezo-modes are directly intersecting the nozzle operation, measures to suppress them are far more effective toward improving the overall performance of the nozzle rather than taking care of ensure that the longitudinal wave is free to operate within the nozzle body without interference from horn modes. Finally it was determined that the difference in performance between comparable symmetric and

asymmetric nozzle designs was due to a longitudinal standing wave set up in the asymmetric nozzles that was not aligned with the longitudinal axis of the nozzle due to being input on only one side of the nozzle, but the the overall magnitude of this effect was negligible.

Because of all of these results it is very clear that, future research focus should rest primarily on the design of the piezoelectric transducers to eliminate the source of these types of modes. Non-longitudinal modes that operate within the piezoelectric transducer have a far more destructive effect in the nozzle as indicated by the harmonic results because they are completely preventing the standing wave of the longitudinal mode from reaching the nozzle body. Once the longitudinal standing wave is setup in the nozzle, direct interference by a horn mode does not effect the harmonic results. Therefore, all further research intending to improve future nozzle designs at higher frequencies will need to address the source of the destructive piezo-modes. I would suggest that in order to realize nozzle designs that give acceptable levels of stress at higher frequencies, a comparison study of different PZT transducer sizes must be undertaken. This can be done by optimizing the Z-normal stress measurement of the simulation by incrementally adjusting the thickness of the piezoelectric elements. At ever higher frequencies, more thought may be required in order to design effective transducer elements, but this is where the focus should primarily be if higher frequency designs are to be realized.

All of these various studies were intended to give a better understanding of the underlying effects the non-longitudinal neighbor modes had on the harmonic results of the nozzle. Due to these studies several independent sources of nozzle degradation where identified. In comparing the presumed effect of these various sources, it was clear that the effect due to non-longitudinal modes focused in the piezoelectric elements was the strongest. Due to these results it is clear that simply matching the frequency of the

piezoelectric element with that of the components of the nozzle body is not sufficient at higher frequencies and further research devoted to directly optimizing these higher frequency transducer elements is the required next step. Overall, this understanding will be useful in future nozzle design at ever higher frequencies in order to realize nozzles that can eventually create droplets on the nano-scale.

Bibliography

[1] S.C Tsai, Y.L Song, C.S. Tsai, Y.F. Chou and C.H. Cheng, Appl Phys. Lett., 2006, 88, 014102, (also Virt. J. Nanoscale Sci. Technol., Jan. 16, 2006)

[2] S.C. Tsai, C.H. Cheng, N. Wang; Y.L. Song, C.T. Lee, C. S. Tsai, *Silicon-based megahertz ultrasonic nozzles for production of monodisperse micrometer-sized droplets*, Ultrasonics, Ferroelectrics and Frequency Control, IEEE Transactions on UFFC, vol.56, no.9, pp.1968-1979, September 2009

[3] C.S. Tsai, R.W. Mao, and S.K. Lin, N. Wang and S.C. Tsai, *Miniaturized Multiple Fourier-Horn Ultrasonic Droplet Generators for Biomedical Applications*, Lab. Chip, 10, 2733-2740, 2010

[4] S.C. Tsai, S.K. Lin, R.W. Mao, and C.S. Tsai, *Ejection of Uniform Micrometer-Sized Droplets from Faraday Waves on a Millimeter-Sized Water Drop* , Physical Review Letters, 108, 154501, April 2012

[5] S.C. Tsai, Y.L. Song, T.K. Tseng, Y.F. Chou, W.J. Chen, and C.S. Tsai, *High Frequency Silicon-Based Ultrasonic Nozzles Using Multiple Fourier Horns*, IEEE Trans. on Ultrasonics/Ferroelectrics and Frequency Control, See Pg. 50, 277-286, 2004.

[6] Shirley S. Tsai, and Chen S. Tsai, *Linear theory on temporal instability of mega-*

hertz faraday waves for monodisperse microdroplet ejection, IEEE Trans. Ultrasonics, Ferroelectrics and Freq Control Vol.60(8), 1746 - 1755 (2013)

[7] C.S. Tsai, R.W. Mao, S.K. L.Y. Zhu, and S.C. Tsai, *Faraday instability-based micro droplet ejection for inhalation drug delivery*, Technology Vol. 2 (1), March 2014

[8] Michael Faraday, *On a peculiar class of acoustical figures and on certain forms assumed by groups of particles upon vibrating elastic surfaces*, Phi. Trans. Roy. Society, London, A52, 299-340, 1831.

[9] R. Lang, *Ultrasonic atomization of liquids*, J. Acoust. Soc. Am., vol. 34, pp. 6-8, 1962.

[10] Lord Rayleigh (J.W. Strutt), *On the crispations of fluid resting upon a vibrating support*, Philosophical Magazine, vol. 16, pages 5058.

[11] E. Eisner, *Design of Sonic Amplitude Transformers for High Magnification*, The Journal of the Acoustical Society of America, vol 35, 9, pg 1367-1377, September 1963

[12] J. Miles, and D. Henderson, Annu. Rev. Fluid Mech., 1990, 22, 143-165.

[13] G.S. Guthart and T. yao-tsu Wu, Proc R. Soc. London, Ser. A, 1991, 434, 435-440.

[14] K. Kumar, Proc. R. Soc. London, Ser. A, 1996, 452, 113-1126.

[15] J.F Maduzia, Fall 2012 Research Report, 1/15/2012.

[16] J.F Maduzia, Winter 2013 Research Report, 4/15/2013.

[17] E.A Cerda, and E.L Tirapegui, Phys. Rev. Lett., 1997, 78, 859-862.

[18] C.L. Goodridge, H.G.E Hentschel and D.P Lathrop, Phys. Rev. Lett., 1999, 82, 3062-3065.

[19] A.J. Yule and Y. Al-Suleimani, Proc. R. Soc. London, Ser. A, 2000, 456, 1069-1085.

[20] K. Kumar, *Linear Theory of Faraday instability in viscous liquids*, Proc. Of Royal Soc. Of London, A452, 113, 1996.

[21] E.A. Cerda and E.L. Tirapegui, *Faraday's instability in viscous fluid*, J. Fluid Mech., 368, 195-228, 1998

[22] S. Ubal, M. D. Giavedoni, and F.A. Saita, *A Numerical Analysis of the Influence of the liquid depth on two-dimensional Faraday waves*, American Institute of Physics , vol 15 # 10, pg 3099-3113, June 2003.

Appendices

A Asymmetric Single Drive Harmonic Data

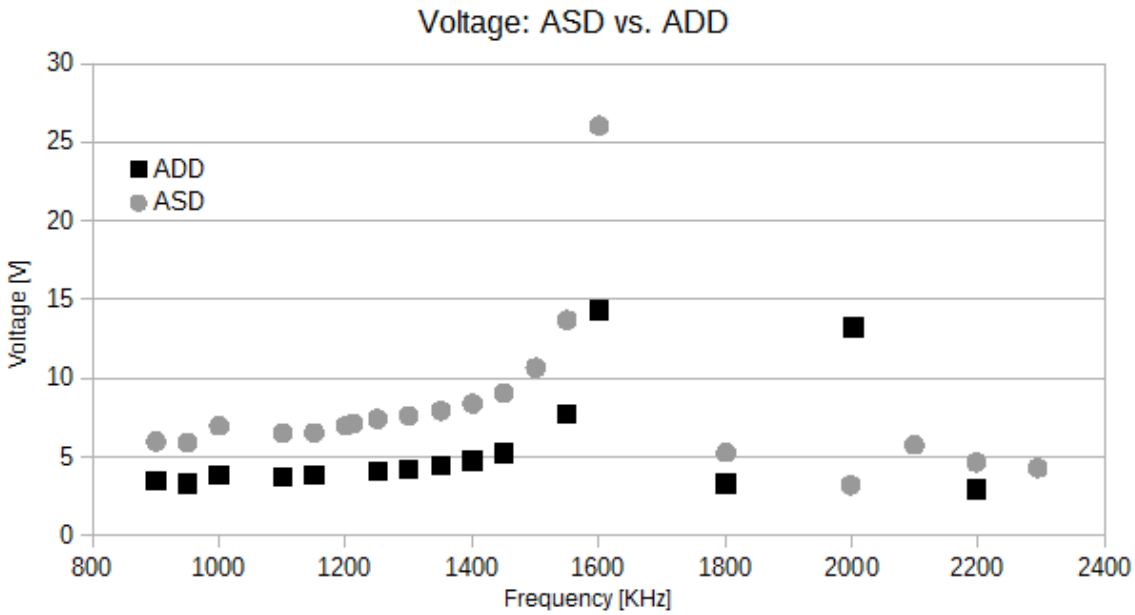

Figure A.1: Single Dual Drive: Voltage

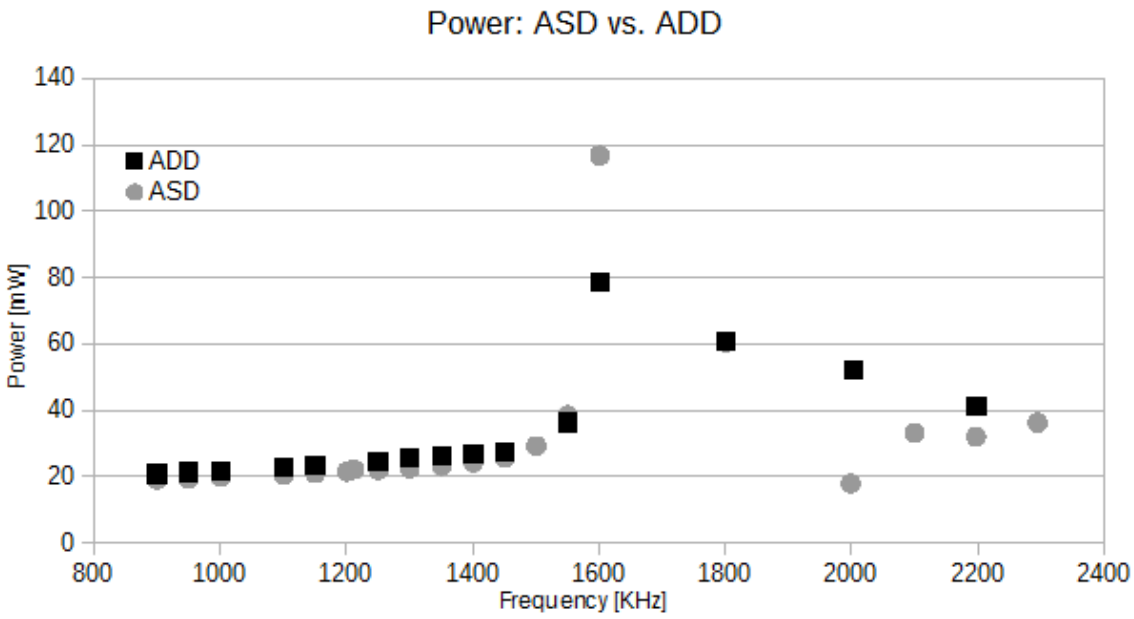

Figure A.2: Single Dual Drive: Power

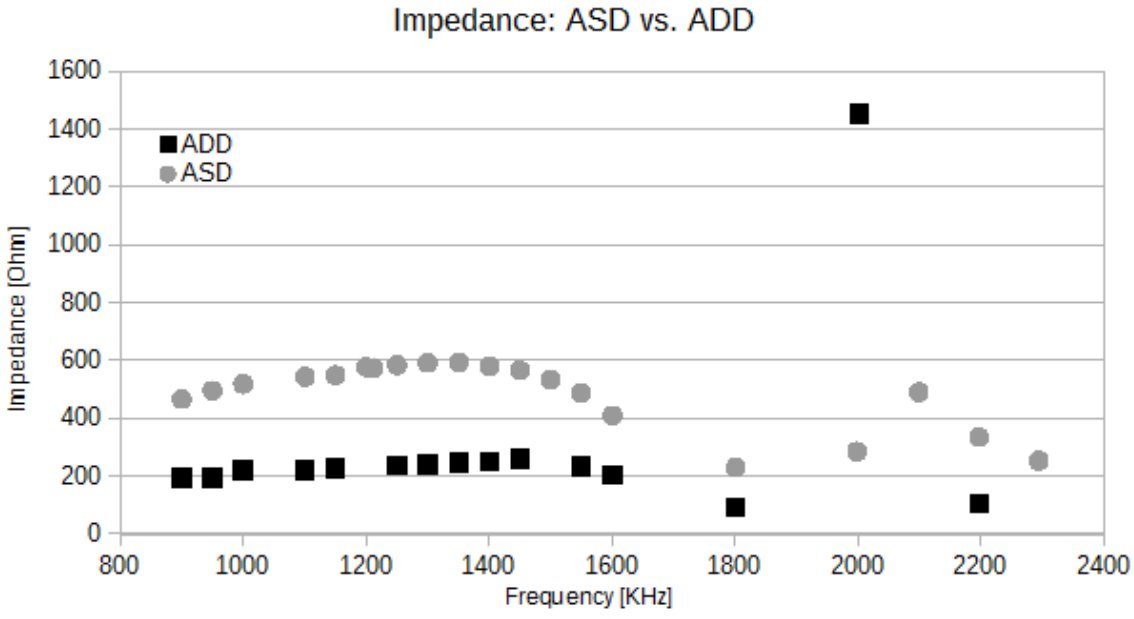

Figure A.3: Single Dual Drive: Impedance

B Significant Non-longitudinal Mode Classes

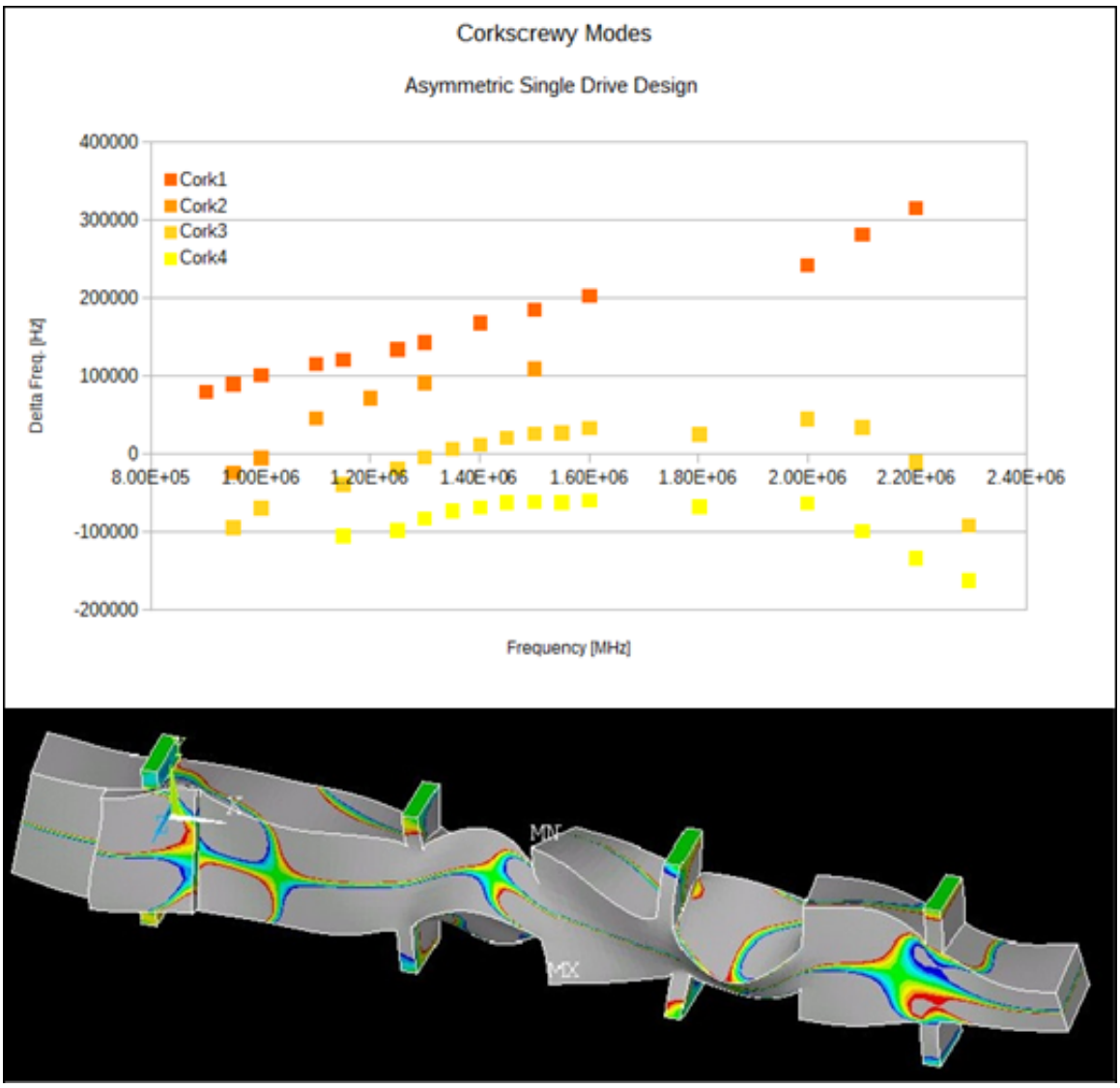

Figure B.4: Corkscrew mode tracks and ANSYS X-Component of Displacement

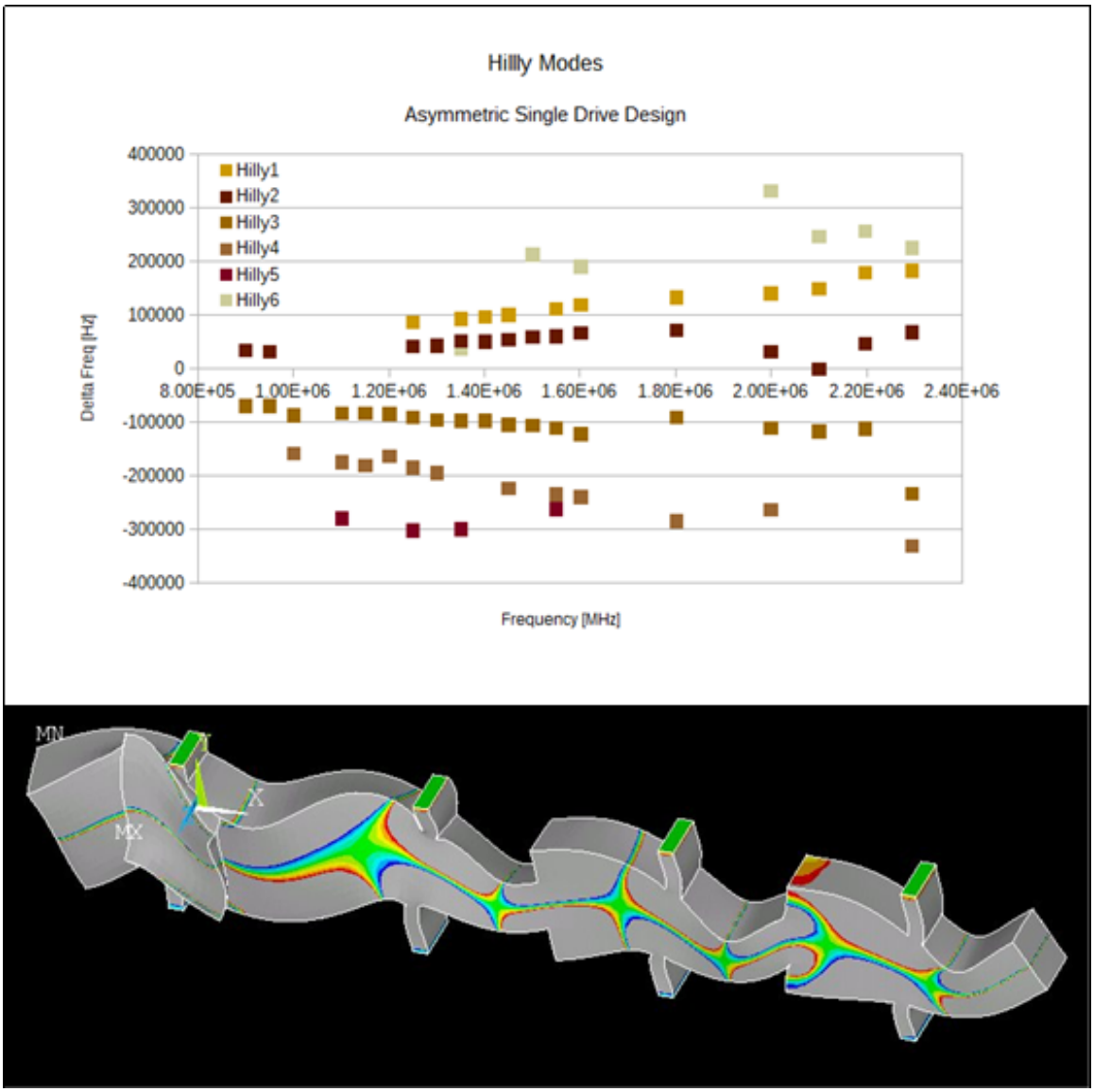

Figure B.5: Hilly mode tracks and ANSYS X-Component of Displacement

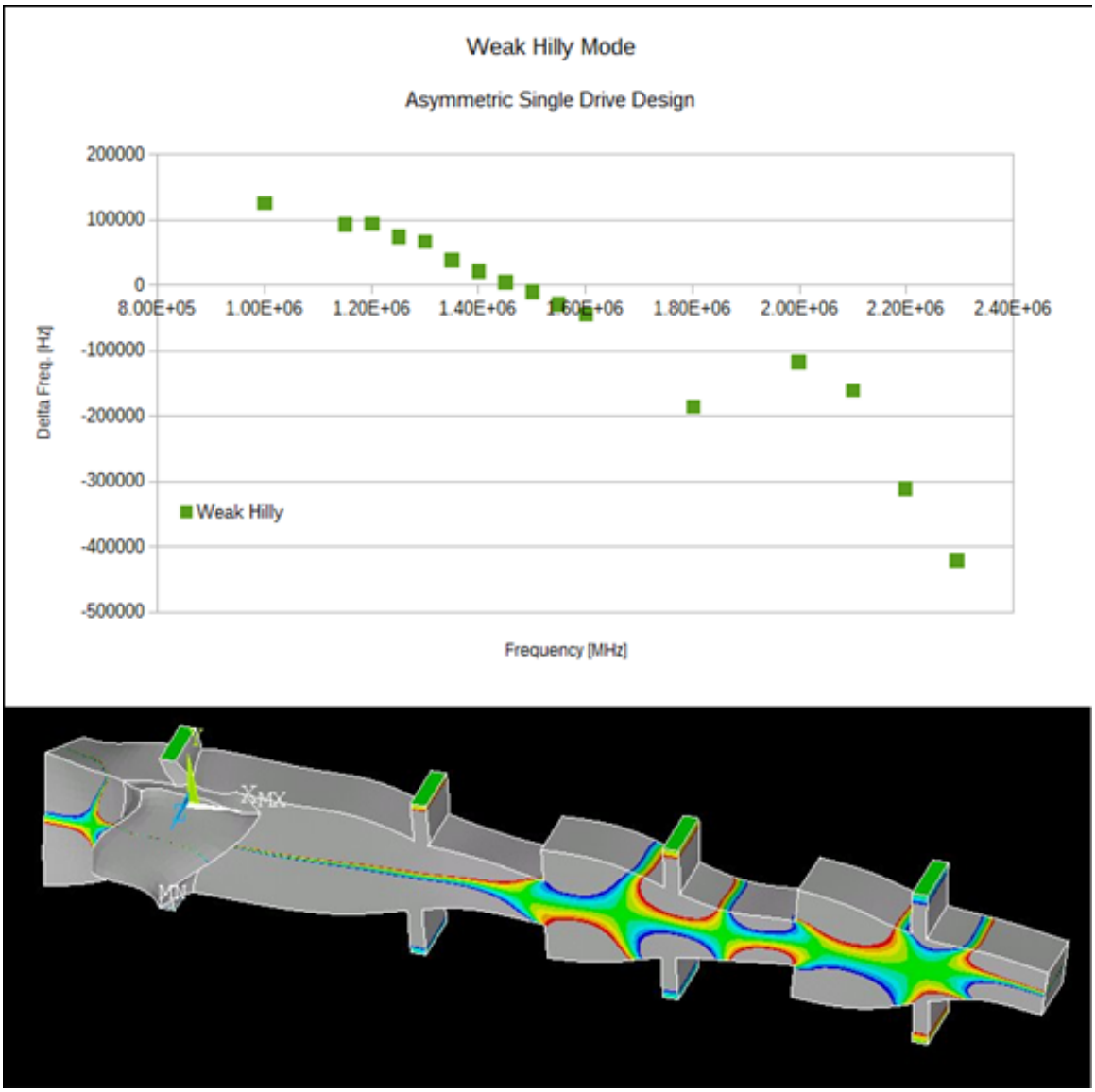

Figure B.6: Slightly Hilly mode tracks and ANSYS X-Component of Displacement

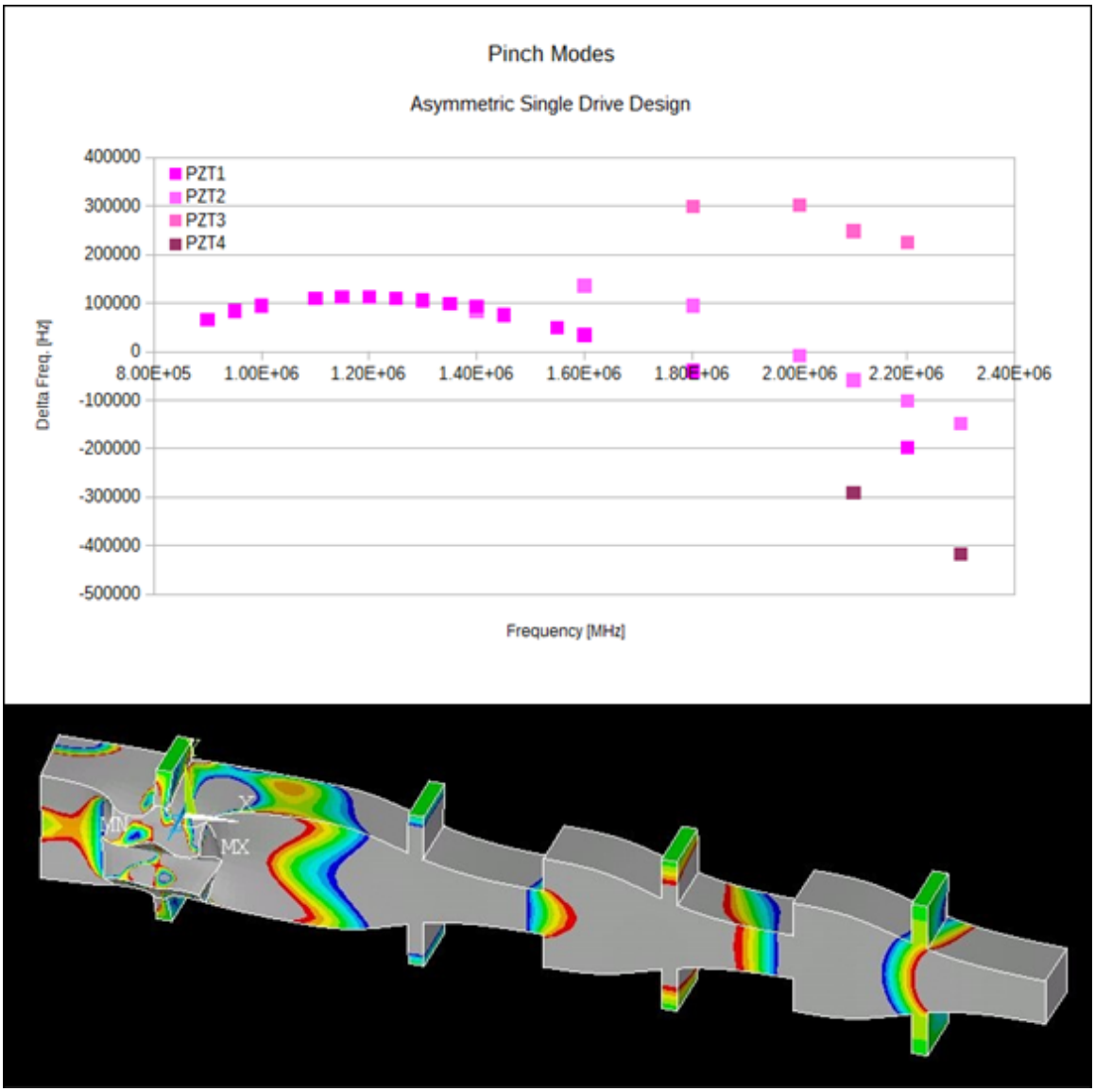

Figure B.7: Pinch mode tracks and ANSYS X-Component of Displacement

C Thick DSNS ASD Comparison Harmonic Data

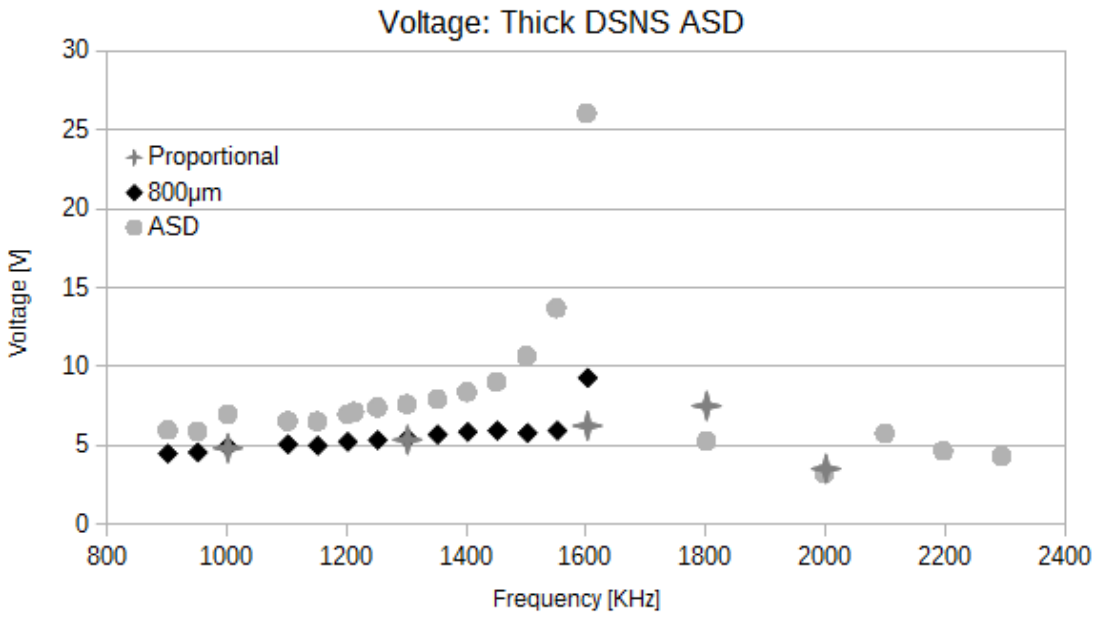

Figure C.8: Single Drive Thick DSNS: Voltage

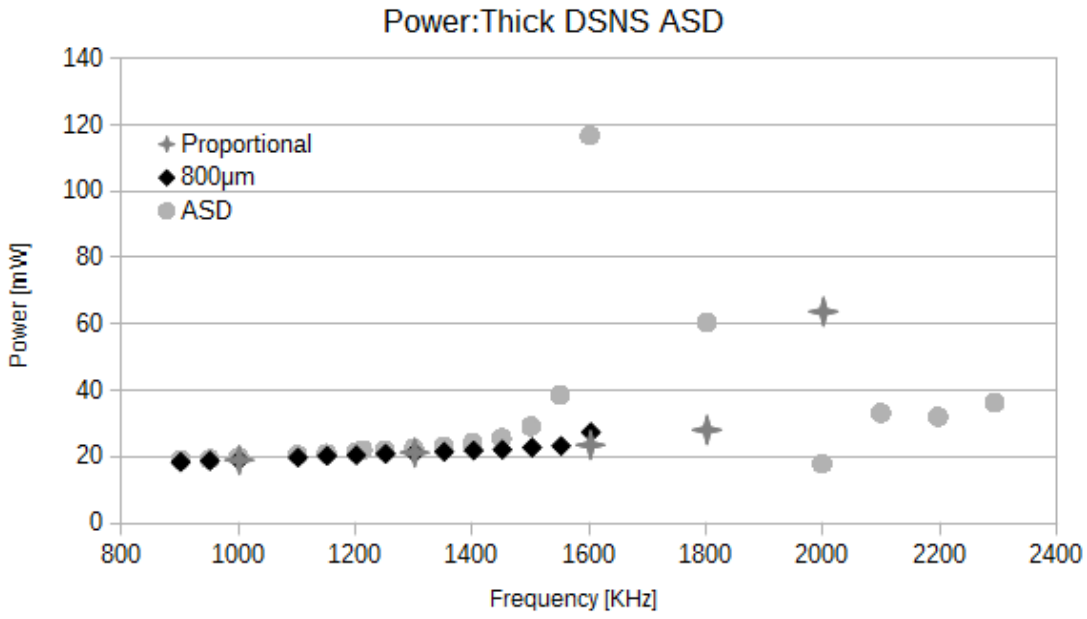

Figure C.9: Single Drive Thick DSNS: Power

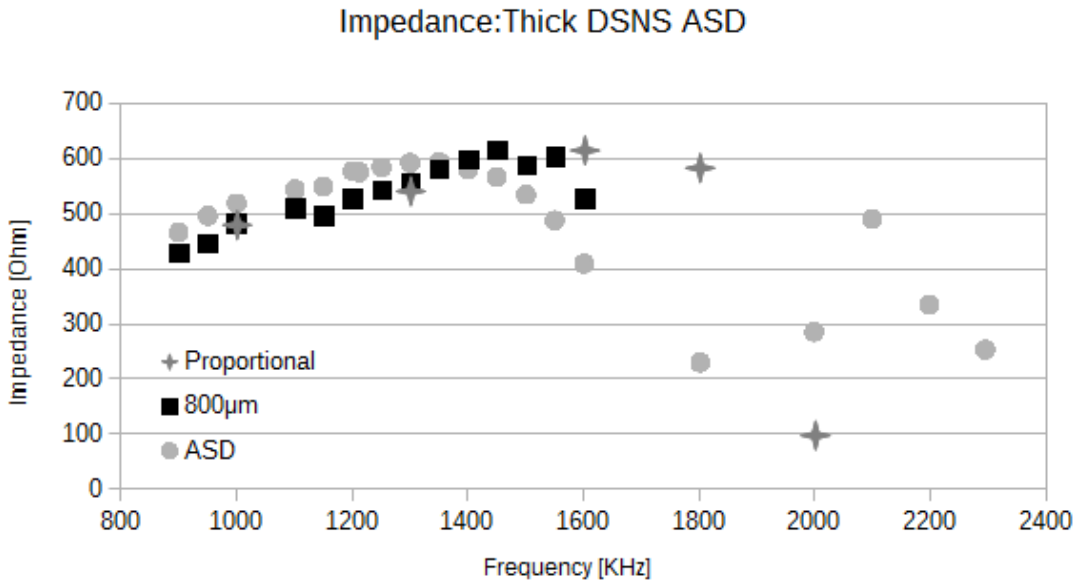

Figure C.10: Single Drive Thick DSNS: Impedance

D Thick DSNS ADD Comparison Harmonic Data

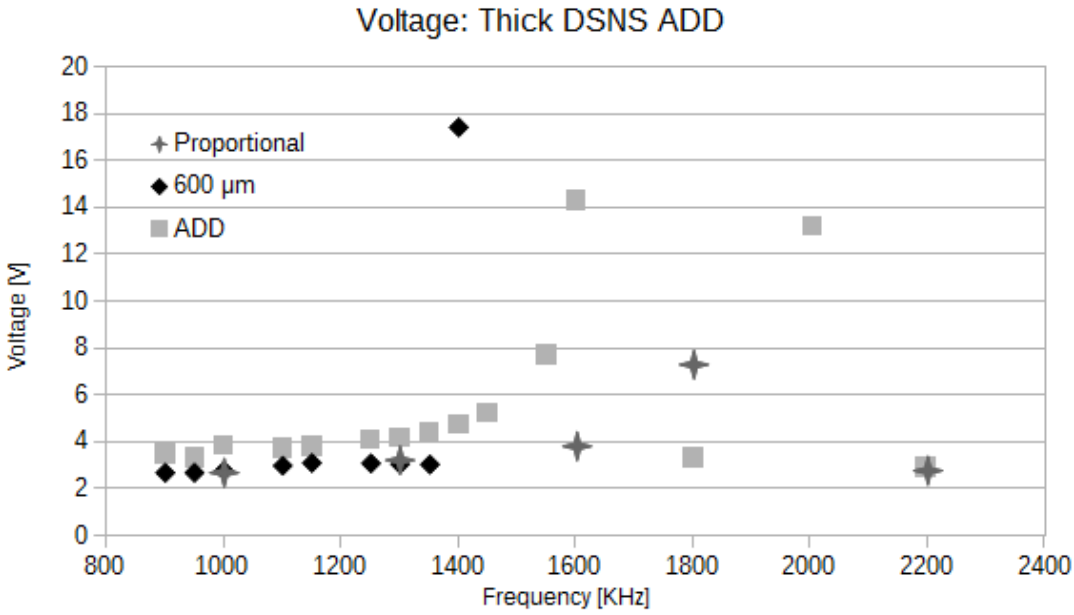

Figure D.11: Dual Drive Thick DSNS: Voltage

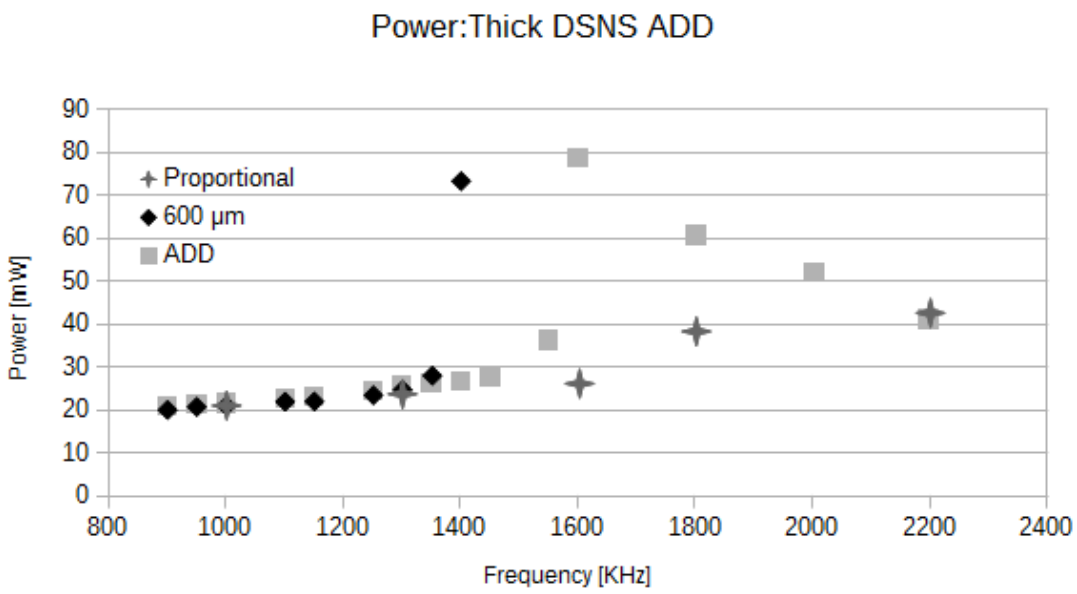

Figure D.12: Dual Drive Thick DSNS: Power

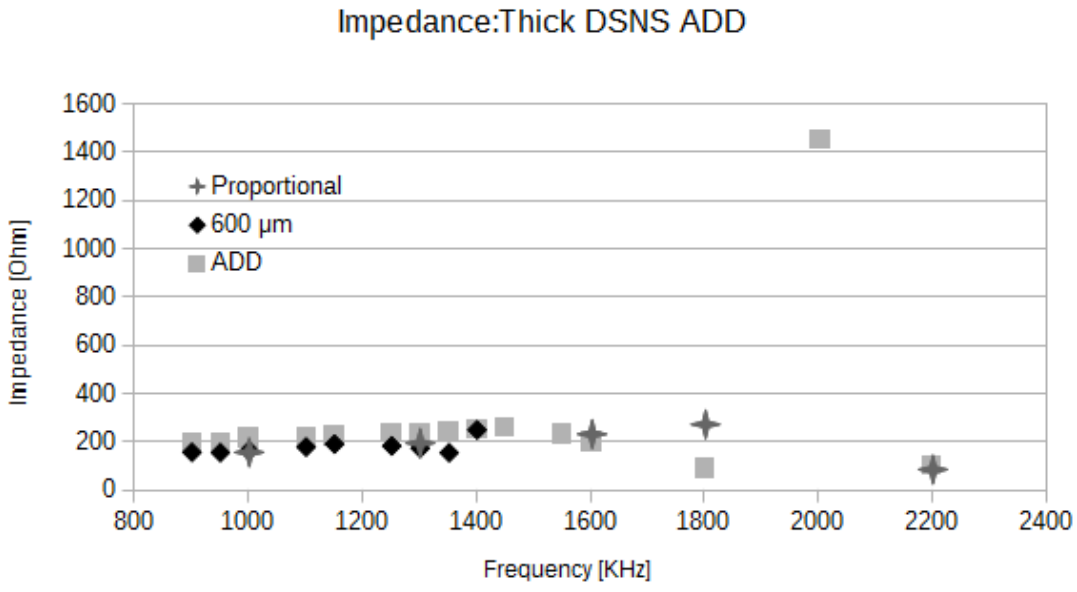

Figure D.13: Dual Drive Thick DSNS: Impedance

E Advanced DSNS Modifictation Harmonic Data

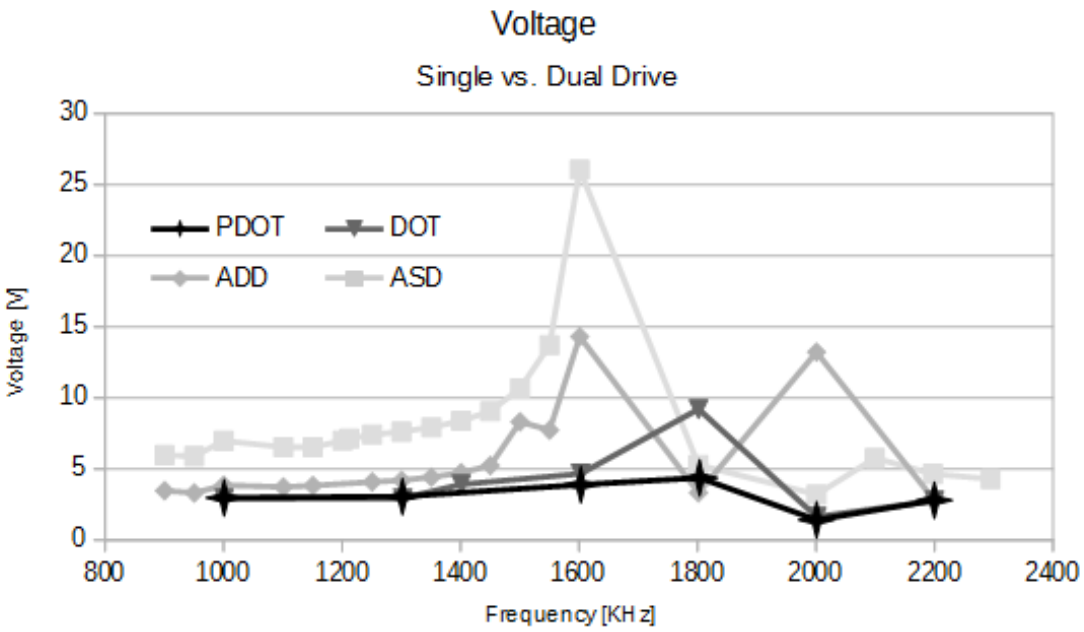

Figure E.14: Modification Harmonic Comparisons: Voltage

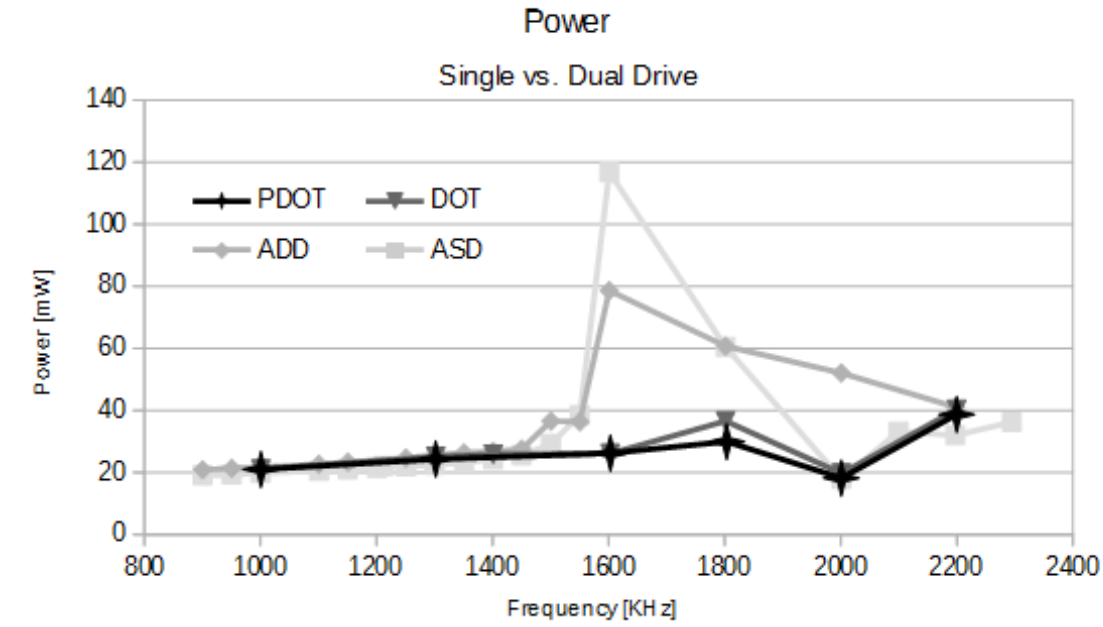

Figure E.15: Modification Harmonic Comparisons: Power

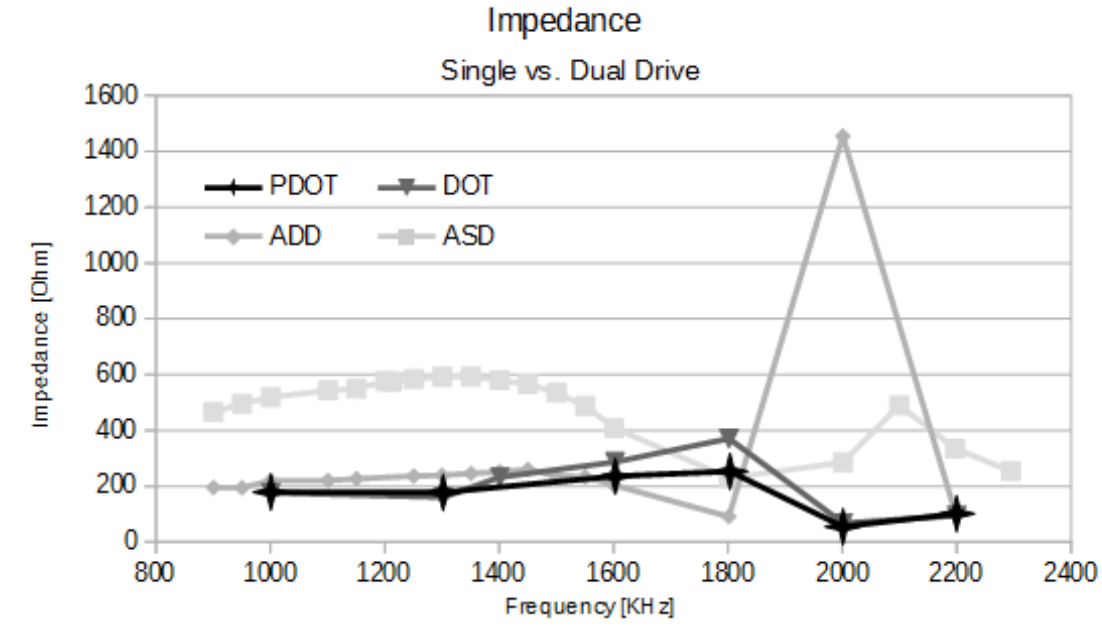

Figure E.16: Modification Harmonic Comparisons: Impedance

F Snakey Mode Modification Shift

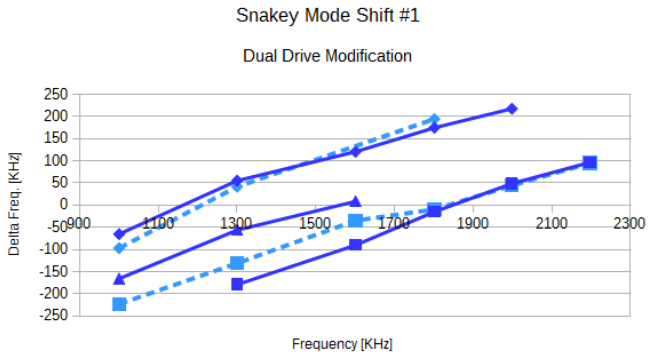

(a) Dual Drive Modification Snakey Mode Shift

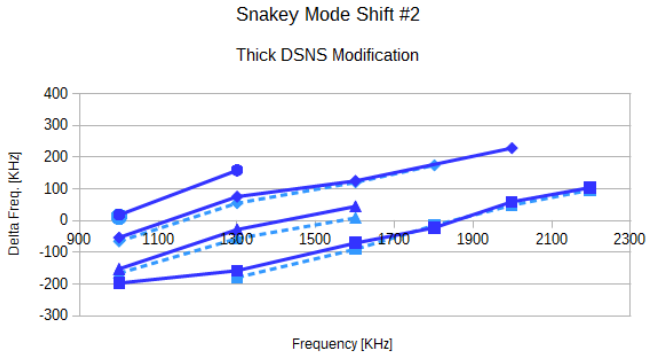

(b) Optimum Thick DSNS Modification Snakey Mode Shift

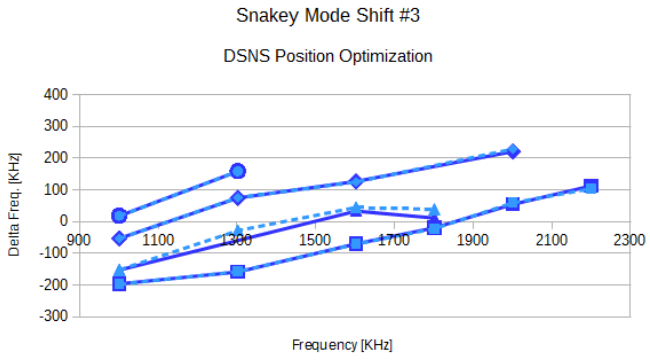

(c) Snakey Modes Shift Dual Drive Modification

Figure F.17: Snakey Mode Shifts Resulting from Nozzle Modifications